NASA CONTRACTOR REPORT

NASA CR-1414

EVALUATION OF CONFIGURATION CHANGES ON OPTIMUM STRUCTURAL DESIGNS FOR A MARS ENTRY CAPSULE

by Gerald A. Cohen

Prepared by
PHILCO-FORD CORPORATION
Newport Beach, Calif.
for Langley Research Center

NATIONAL AERONAUTICS AND SPACE ADMINISTRATION • WASHINGTON, D. C. • AUGUST 1969

NASA CR-1414

EVALUATION OF CONFIGURATION CHANGES ON OPTIMUM STRUCTURAL DESIGNS FOR A MARS ENTRY CAPSULE

By Gerald A. Cohen

Prepared under Contract No. NAS 1-5554-5 by
PHILCO-FORD CORPORATION
Newport Beach, Calif.

for Langley Research Center

NATIONAL AERONAUTICS AND SPACE ADMINISTRATION

For sale by the Clearinghouse for Federal Scientific and Technical Information
Springfield, Virginia 22151 – CFSTI price $3.00

PREFACE

This study was initiated while the author was employed by the Philco-Ford Corporation. Technical responsibility for the completion of the work and the preparation of this report resides in Structures Research Associates under subcontract to Philco-Ford. The contribution of Charles G. Dietz, who assisted in the analysis, and James R. Dowty, who provided design support, is gratefully acknowledged.

ABSTRACT

Optimum structural designs for Martian entry capsules are obtained for 140^{o} blunted cone, 60^{o} spherical dish, and 0A.65 tension shell configurations. These designs have 19 foot base diameters and are based on theoretical pressure and convective heat transfer distributions for orbit mode entry with a ballistic coefficient of 0.32 slug/ft^2.

CONTENTS

EVALUATION OF CONFIGURATION CHANGES

ON

OPTIMUM STRUCTUAL DESIGNS FOR A MARS ENTRY CAPSULE

by

Gerald A. Cohen

Structures Research Associates, Newport Beach, California

SUMMARY

Optimized capsule designs have been obtained for 140° blunted cone, 60° spherical dish, and OA.65 tension shell geometries. These designs are based on theoretical pressure and convective heat transfer distributions for an out-of-orbit Martian entry trajectory with a ballistic coefficient of 0.32 slug/ft^2. The designs presented are optimum in the sense that structural weight has been minimized with respect to buckling failure of the capsule. As is consistent with the shroud limitation of the Saturn V booster, the designs have 19 foot base diameters. Structure and heat shield weights are based on a backface temperature of approximately 300°F, which has been shown in a previous study to be the optimum temperature. For the conical and spherical geometry, sandwich construction is treated, whereas ring-stiffened construction is considered for the tension shell.

Comparison of the designs obtained reveals that for these configurations the structure plus heat shield weights vary as their drag coefficients. However, since in each case this weight is a relatively small percentage ($\approx$11%) of the total entry weight, for the given size and ballistic coefficient the residual weights available for landed payload vary also as the drag coefficients. The residual weights obtained are 4828, 4382, and 4065 lb for the OA.65 tension shell, 140° cone, and 60° spherical dish, respectively. It is noted, however, that the flow field analysis did not allow for the possibility of flow separation, which is likely during a significant portion of the tension shell entry trajectory. Consequently, the high drag coefficient indicated for the tension shell may not be achieved, so that the residual weight obtained for it cannot be considered as reliable as those obtained for the other configurations.

INTRODUCTION

In Reference 1 are presented optimum design procedures for lightweight, low ballistic coefficient Martian entry capsules for both sandwich and ring-stiffened aeroshells. These procedures were used in that study to obtain optimized capsule designs and the associated structural and heat shield weights for 120° cone and 0A.833 tension shell geometries.

The present study makes use of the same procedures to evaluate three additional blunt configurations, viz., a 140° cone, a 60° spherical dish, and an 0A.65 tension shell. The greater drag coefficients of these configurations (Ref. 1) permit an increase in entry weight, for a given ballistic coefficient, over those for the previously studied configurations. The optimized designs presented are based on sandwich wall construction for the 140° cone and shperical dish, and ring-stiffened construction for the 0A.65 tension shell. In addition to subjecting each trial design to stability and stress analysis, fundamental free vibration modes of finalized designs were obtained for several harmonics, including the harmonic for which the fundamental frequency attains a minimum value.

SYMBOLS

C	general instability correlation factor
C_D	drag coefficient
E	Young's modulus, psi
h	thickness of Z-section interior ring, in.
ℓ	ideal cross section perimeter of Z-section interior ring, in.
m, n	empirical exponents for spherical dish instability correlation
N	circumferential harmonic number
R	cross-sectional radius of tubular base ring, in.
r	shell attachment radius for interior ring, in.

r_B	capsule base radius, in.
s	meridional distance from spherical nose, in.
T	shell stress resultant, lb/in.
t	base ring thickness, in.
t_c	sandwich core thickness, in.
t_f	sandwich face sheet thickness, in.
W	weight, lb
W_E	total entry weight, lb
W_R	residual weight, $W_E - W_S$, lb
W_S	total structure plus heatshield weight, lb
x	axial distance from tension shell base, in.
y	radial distance from axis of revolution, in.
β	ballistic coefficient, slug/ft^2
Δ	increase in riveted flange width necessary to accommodate a rivet, in.
λ	load factor
λ_{SF}	stability safety factor

RESULTS

In Figure 1 are shown the three configurations considered. Optimized structural designs were obtained for these configurations using the analytical procedures of Reference 1, and only the final results are presented here. Each capsule is designed for a 19 foot base diameter and a ballistic coefficient of 0.32 slug/ft^2. Consequently, the total entry weights are determined by the drag coefficients (Fig. 1). The designs are based on the theoretical pressure loading and convective heat transfer distributions presented in Reference 1. As in Reference 1, the desired buckling factor

of safety is $\lambda_{SF} = 2.25$, i.e., (in the absence of structural imperfections) the designs should buckle at 2.25 times the expected entry load. However, in order to limit the number of design iterations, variations of ± 0.25 from this value were considered acceptable. The payload attachment radius is 35% of the base radius, and the ratios of spherical nose radius to base radius are 0.25, 2.0, and 0.3 for the cone, spherical dish, and tension shell, respectively. The design material is aluminum.

The free vibration analysis made use of the computer program described in Reference 2. It is noted that in the calculation of axisymmetric (N = 0) and antisymmetric (N = 1) free vibration modes the residual mass associated with the payload and capsule nose section has been lumped in the payload ring. On the other hand for higher harmonic (N > 1) modes, in which it is doubtful that the payload mass participates, the estimated payload mass has been neglected.

The essential elements of the 140° sandwich cone and 60° sandwich spherical dish designs are presented in Table I, and those for the ring-stiffened tension shell in Table II. Given in parentheses after the critical load factors are the corresponding circumferential wave numbers. It is noted that for both sandwich designs, the sandwich face sheets are minimum gage.

140° Sandwich Cone

The prebuckling state, buckling modes, and stress response for the 140° sandwich cone are shown in Figures 2 through 6. In these and succeeding figures, meridional distance is measured from the spherical nose, and the curves start at the payload ring and terminate at the base ring. Note that the designs are based on a nominal buckling safety factor of 2.25 to allow for discrepancies between stability theory and experiment, whereas the stress magnitudes shown are for the usual safety factor of 1.5. Figures 2 through 6 exhibit the same general characteristics as the corresponding curves for the 120° sandwich cones of Reference 1. On the other hand, in contrast to the 120° cones, it was found that the nonlinearity of the prebuckling state is not negligible for the 140° cone. It has the beneficial effect of increasing the buckling load by roughly 25 percent.

Figures 7 through 11 show the fundamental vibration modes for the 140° sandwich cone for circumferential harmonics 0 through 4, respectively. As is typical for entry capsules, the minimum natural frequency, 13.1 cps, occurs in an approximately inextensional mode with two circumferential waves. This mode shape (Fig. 9) is characteristically (for cones) linear and is very similar to the N = 2 buckling mode.

60° Sandwich Spherical Dish

The design step for the sandwich spherical dish is essentially the same as that for sandwich cones (Ref. 1) except that in this case the general instability correlation [Eq. (3) of Ref. 1] was changed to

$$\lambda = CEt_f^{\,m} t_c^{\,n}$$

where the correlation parameters C, m, and n are adjusted as the design progresses in accordance with the stability analysis computer runs. The prebuckling state, buckling modes, and stress response for the 60° sandwich spherical dish are shown in Figure 12 through 16. These response curves are suprisingly similar to the corresponding curves for the sandwich cone. One significant difference is the intensity of stress in the outer sandwich layer in the vicinity of the payload ring. Figure 16 indicates a hoop stress of 109 000 psi at the payload ring of the spherical dish, whereas Figure 6 indicates a corresponding hoop stress of only 84 000 psi for the cone.* Because of uncertainties in the payload stiffness, which was neglected, these are not precise values. However, they are indicative of the possible need for local modifications of the shell near the payload ring.

Figures 17 through 21 show the fundamental vibration modes for the spherical dish for circumferential harmonics 0 through 4, respectively. The minimum natural frequency, 12.6 cps, is very close to the value, 13.1 cps, obtained for the 140° cone.

OA.65 Ring-Stiffened Tension Shell

In Table II are presented the elements of the ring-stiffened tension shell design. As with the OA.833 tension shell designs of Reference 1, stringers are used to suppress large prebuckling deformations.

The prebuckling state, buckling modes and stress response for the OA.65 tension shell are shown in Figures 22 through 26. As is typical for tension shells, the buckling mode (Fig. 23) is essentially confined to the shallow base region, where the hoop compressive stress resultant is greatest (cf. Fig. 22). Superimposed on Figure 23 is the interior ring mass distribution of the design. As explained in Reference 1, this distribution deviates from the buckling mode shape because of the imposition of riveted flange constraints in the design program. These constraints typically have their greatest effect near the base of the shell.

---

* The sandwich core shear stress at the payload ring is correspondingly higher for the spherical dish (200 psi) than it is for the cone (87.5 psi).

Note that the meridional stress at the stringer centroid is shown in Figure 25 along with the shell stresses at the inner face of the skin. Comparison of Figures 25 and 26 with Figures 5, 6, 15, and 16 shows that, except in the vicinity of the payload ring, the tension shell stress levels are lower than those for the sandwich aeroshells.

The base ring for the tension shell is heavily loaded relative to those for the sandwich cone and spherical dish. Thus, whereas the base rings for the sandwich cone and spherical dish are not local stability limited, the stability limit of the tension shell base ring coincides approximately with the imposed design limit of R/t = 125.

Figures 27 through 31 show the fundamental vibration modes for the OA.65 tension shell for circumferential harmonics 0 through 4, respectively. The minimum natural frequency, 8.53 cps, is considerably smaller than the natural frequencies of the 140° cone and 60° spherical dish. In contrast to the fundamental N = 2 vibration modes for the other designs, this mode (Fig. 29) does not have its maximum amplitude at the base ring. Therefore, it is not expected that the corresponding frequency would be strongly affected by variations in the base ring stiffness. On the other hand, since in this mode there is significant normal vibration at the payload ring, the unknown stiffness of the payload itself, which was neglected in the calculation, may have a significant effect on the frequency.

Configuration Comparison

Summarized in Table III are the total structure plus heat shield weights W_S, total entry weights W_E, corresponding weight fractions and residual weights W_R for each design obtained. In addition, the drag coefficients upon which the total entry weights are based are shown. For the purpose of comparison, these values for the corresponding (0.32 slug/ft^2, 300°F) configurations of Reference 1 are also shown.*

It is seen that the three designs of the present study show considerably better performance than do the designs of Reference 1. However, the differences in total structure plus heat shield weights are not great, the primary differences being in total entry weights, which, for the given ballistic coefficient and base diameter, are directly proportional to the average drag coefficient. Since, as noted in Reference 1, flow separation, which probably would occur on the tension shell capsules, has been neglected in the calculation of C_D, the total entry weights computed for the tension shell capsules cannot be considered reliable.

*It is noted that the designs of Reference 1 were subjected to angle-of-attack loading conditions (associated with a hypothetical attitude control failure) which are probably somewhat more severe than the axisymmetric conditions used for the present designs.

Detail Drawings of Optimized Designs

Design layout drawings were prepared to illustrate typical mechanical details of the various structural concepts as they applied to the three aeroshell geometries.

140° sandwich cone.- Figure 32 shows a preliminary design layout for a 140° cone of sandwich construction. The basic structural components in this concept are the shell assembly, the base ring and the payload mounting ring. It is anticipated that the shell will be assembled in two principal stages. The nose section including the payload mounting ring would be layed up on a male mold, bagged, and cured. This subassembly would then be incorporated into the rear shell structure in a second lay-up operation on a conical male mold. The base ring would subsequently be assembled to this shell assembly with conventional structural fasteners. The base ring is attached to the shell with attach doublers and tube supports. These members are disposed in a manner which will most effectively react the tension loads of the shell.

The principal materials in this assembly are 7075-T6 aluminum alloy for the sandwich face sheets, payload mounting ring and base ring; 5052 aluminum alloy bonded core with a density of 5.2 lb/ft^3, and adhesive HT424 (Bloomingdale Rubber Company) sandwich bond.

60° spherical dish.- Figure 33 shows a preliminary design layout for a spherical dish of sandwich construction. In this configuration the methods of fabrication are essentially the same as for the honeycomb sandwich cone. Due to the double curvature of the shell, however, the shell facing segments must be shaped by stretch forming before assembly. Other details of the assembly and material selections are the same as for the sandwich cone.

OA.65 tension shell.- Figure 34 shows a ring and stringer-stiffened design for the OA.65 tension shell. The tension shell shape does not extend forward of the payload ring. Shell sections could be die-formed and welded together to form the complete shell. Roll formed rings and stringers would be located in an assembly fixture and the welded shell assembly would be riveted to these stiffeners. As in the previous designs, the base ring is attached to the shell assembly with a series of doublers and supports. Where the stringer depth permits, they are notched to fit over the stiffening rings. Where the depth of the rings approaches the depth of the stringers, the stringers are discontinuous over the ring. Materials for this capsule are 7039 aluminum alloy for the shell and base ring, and 7075 alloy for the stiffeners and payload mounting ring. Dimensions and locations of the stiffening rings are tabulated in Table IV.

CONCLUDING REMARKS

Optimized Martian entry capsule designs have been presented for three geometric aeroshell configurations which are more blunt than those heretofore considered. These designs, 140^{o} sandwich cone, 60^{o} sandwich spherical dish, and the 0A.65 ring-stiffened tension shell have a 19 foot base diameter and are based on orbit mode entry with a ballistic coefficient of 0.32 slug/ft^2. The designs obtained show significant improvement in performance over corresponding designs presented in Reference 1 for 120^{o} cone and 0A.833 tension shell capsules.

The 0A.65 tension shell configuration requires a somewhat greater structure plus heat shield weight than does either the 140^{o} cone or spherical dish. Therefore, the attractiveness of the tension shell configuration is primarily due to its higher drag coefficient, which for a given ballistic coefficient allows a significantly larger total entry weight. The larger total entry weight of the tension shell more than compensates for its greater structural weight requirement, thereby resulting in the largest residual weight (4828 lb) available for landed payload. However, as noted in Reference 1, because for the tension shell there are extensive regions of positive pressure gradient in the shock layer, it is probable that, due to flow separation, the high drag result will be degraded over major portions of the entry trajectory. Because of this uncertainty, the residual weight presented for the tension shell capsule should be viewed only as an upper bound value.

Because of this uncertainty in the tension shell designs, the 140^{o} sandwich cone, having a residual weight of 4382 lb, appears to be the most efficient configuration studied. Based on the results of Reference 1, since this design has minimum gage face sheets, one would expect that it could be improved further by employing ring-stiffened construction.

REFERENCES

1. Cohen, G. A.; Foster, R. M.; and Dowty, J. R.: Synthesis of Optimum Structural Designs for Conical and Tension Shell Mars Entry Capsules. NASA CR-1365, 1969.

2. Cohen, G. A.: Computer Analysis of Asymmetric Free Vibrations of Ring-Stiffened Orthotropic Shells of Revolution. AIAA J., vol. 3, no. 12, December 1965, pp. 2305-2312.

TABLE I

SANDWICH DESIGNS

		140^{o} Cone	60^{o} Spherical Dish
(1)	Stability Safety Factor		
	λ_{SF} = 2.08(2)		2.04(2)
	= 1.95(5)[a]		2.10(7)
(2)	Shell Aft of Payload Ring[b]		
	t_c = 0.912 in.		0.860
	t_f = 0.016 in.		0.016
	W = 282 lb		280
(3)	Base ring[c]		
	t = 0.039 in.		0.035
	R = 4.81 in.		4.37
	W = 109 lb		93
(4)	Payload Ring		
	W = 19 lb		16
(5)	Heat Shield		
	W = 119 lb		90
(6)	Nonusable Entry Weight[d]		
	W = 568 lb		515
(7)	Total Entry Weight		
	W = 4950 lb		4580

[a] The sandwich designs were originally obtained for an assumed room temperature value of Young's modulus, E = 10.3 x 10^6 psi. In order to be consistent with a structural temperature of 300°F, upon which the heat shield weights are based, the response variables of these designs were adjusted to account for a reduction in E to the value 9.35 x 10^6 psi. In so doing, the stability safety factor for the 140^{o} cone fell slightly below the specified range of 2.0 - 2.5.

[b] Includes 0.1 lb/ft^2/face sheet adhesive weight and weight allowance for splices.

[c] Includes weight allowance for sandwich closure and tube support.

[d] Includes allowance for nose section.

TABLE II

OA.65 TENSION SHELL DESIGN

(1) Stability Safety Factor
λ_{SF} = 2.21(2)
= 2.50(14)

(2) Unstiffened Shell Aft of Payload Ring[a]
t = 0.046 in.
W = 190 lb

(3) 26 Interior Rings[b]
W = 61 lb

(4) 90(.5 × .75 × .1 × .016) Full Length Stringers[b]
W = 21 lb

(5) Base Ring[c]
t = 0.044 in.
R = 5.50 in.
W = 123 lb

(6) Payload Ring
W = 8 lb

(7) Heat Shield
W = 160 lb

(8) Nonusable Entry Weight[d]
W = 597 lb

(9) Total Entry Weight
W = 5425 lb

---

[a] Includes weight allowance for ring-stringer fasteners.

[b] Includes allowance for rivet weight.

[c] Includes weight allowance for tube support.

[d] Includes allowance for nose section.

TABLE III

COMPARISON OF VARIOUS CONFIGURATIONS

FOR β = 0.32 SLUG/FT^2 (ORBIT ENTRY)

Configuration	W_S(lb)	W_E(lb)	W_S/W_E	C_D	W_R
OA.65 Tension shell	597	5425	.110	1.86	4828
60° Sandwich spherical dish	515	4580	.112	1.57	4065
140° Sandwich cone	568	4950	.115	1.70	4382
OA.833 Tension shell[a]	605	5200	.116	1.78	4595
120° R. S. cone[a]	559	4400	.127	1.51	3841
120° Sandwich cone[a]	585	4400	.133	1.51	3815

[a] from Reference 1

TABLE IV

RING LOCATIONS & DIMENSIONS, IN.

OA.65 TENSION SHELL

RING NO.	r	Δ	ℓ	h	NEXT LARGEST STANDARD GAUGE
1	51.84	.1842	1.421	.0172	.020
2	59.85	.1791	1.444	.0175	↓
3	65.78	.1776	1.451	.0179	↓
4	70.52	.1747	1.464	.0186	↓
5	74.40	.1770	1.453	.0196	↓
6	77.65	.1815	1.433	.0202	.025
7	80.51	.1854	1.416	.0209	↓
8	83.05	.1915	1.388	.0215	↓
9	85.35	.1986	1.357	.0219	↓
10	87.47	.2062	1.322	.0222	↓
11	89.45	.2128	1.292	.0222	↓
12	91.36	.2191	1.264	.0220	↓
13	93.21	.2254	1.235	.0217	↓
14	95.01	.2352	1.192	.0217	↓
15	96.70	.2471	1.138	.0215	↓
16	98.39	.2563	1.096	.0216	↓
17	100.0	.2647	1.059	.0205	↓
18	101.7	.2722	1.025	.0201	↓
19	103.2	.2828	.977	.0198	.020
20	104.7	.2913	.939	.0197	.020
21	106.1	.2952	.921	.0201	.025
22	107.5	.3007	.897	.0205	↓
23	108.7	.3068	.869	.0209	↓
24	109.9	.3144	.835	.0214	↓
25	110.9	.3220	.801	.0220	↓
26	111.9	.2826	.978	.0271	.032

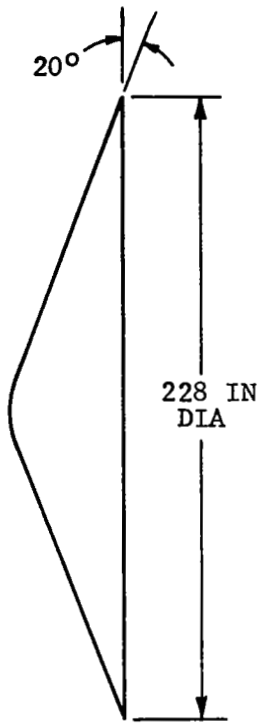

BLUNT CONE, C_D = 1.70

HONEYCOMB SANDWICH STRUCTURE

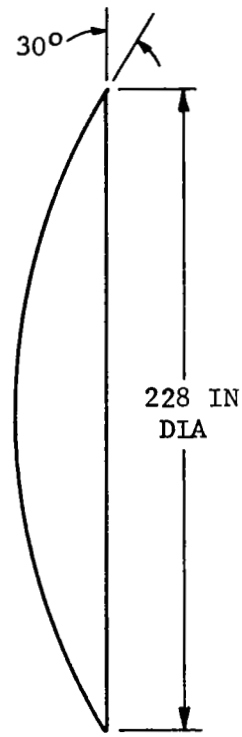

SPHERICAL DISH, C_D = 1.57

HONEYCOMB SANDWICH STRUCTURE

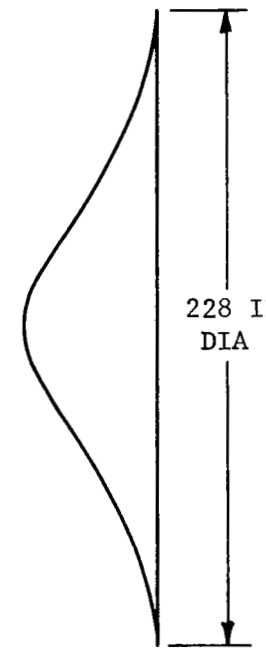

0A.65 TENSION SHELL, C_D = 1.86

RING-STIFFENED STRUCTURE

FIGURE 1. AEROSHELL CONFIGURATIONS

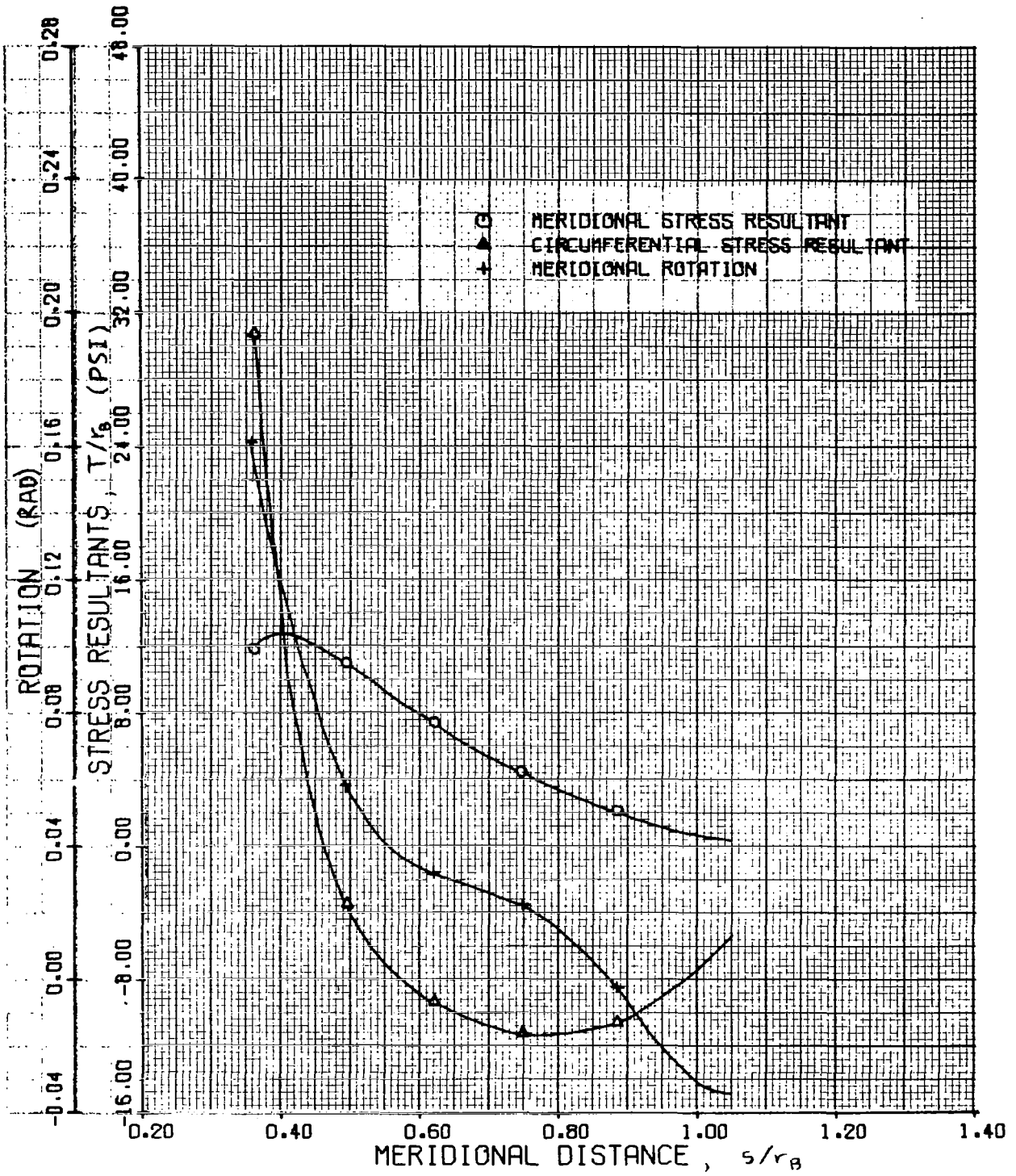

FIGURE 2. PREBUCKLING STRESS RESULTANTS AND ROTATION
140 DEG SANDWICH CONE, S.F. =2.25

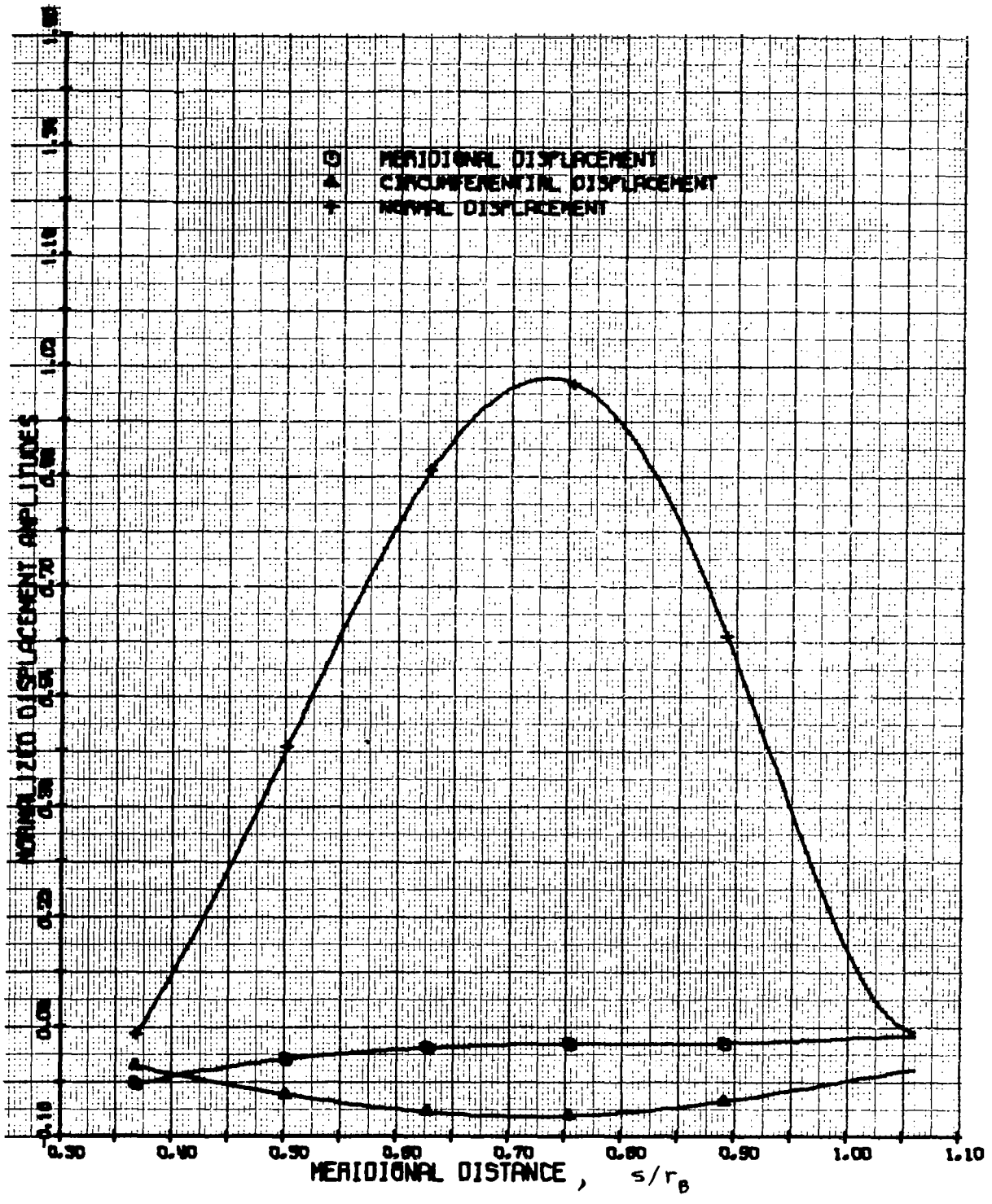

FIGURE 3. BUCKLING MODE DISPLACEMENTS
140 DEG SANDWICH CONE (N=5) S.F. = 1.95

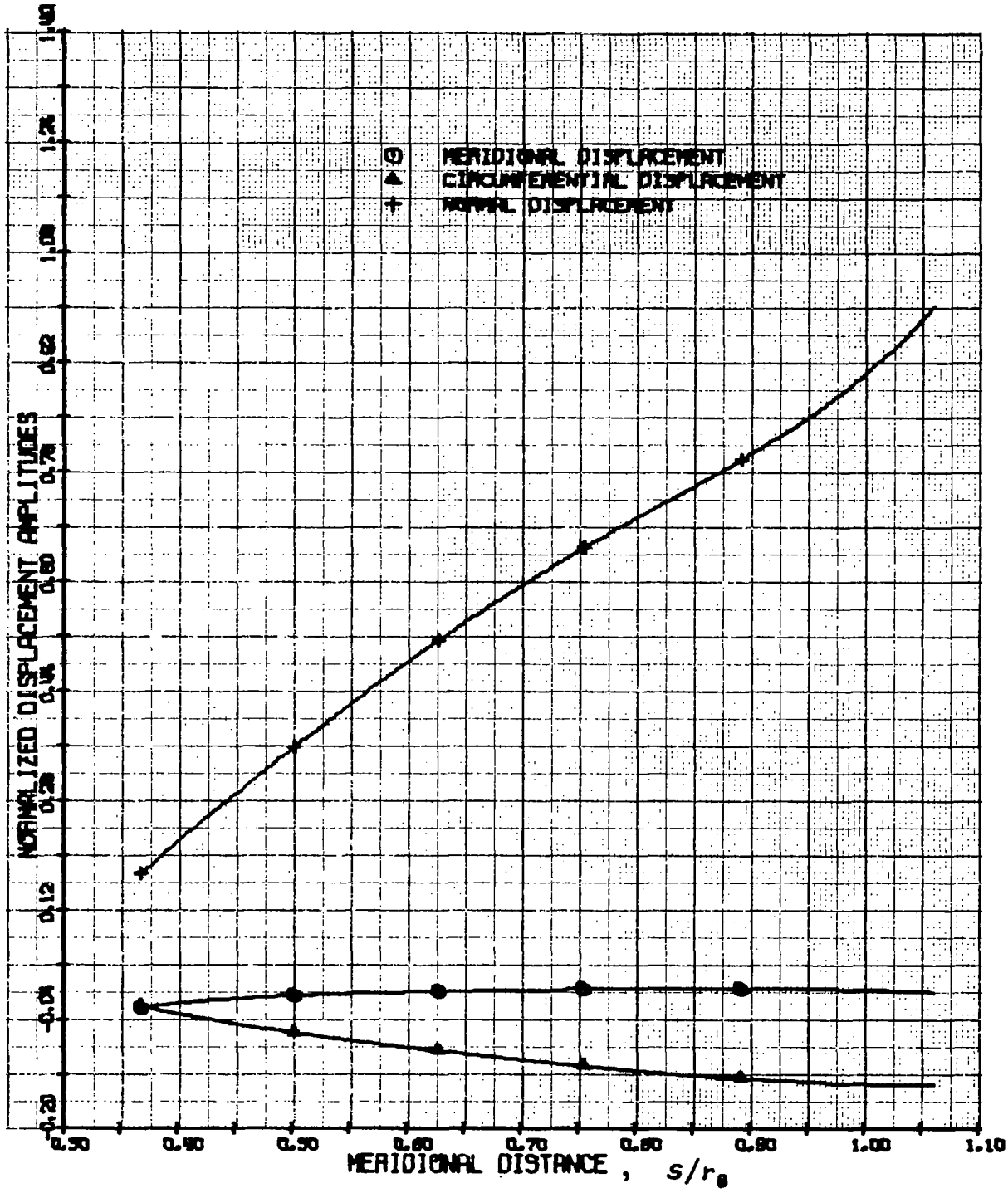

FIGURE 4. BUCKLING MODE DISPLACEMENTS
140 DEG SANDWICH CONE (N=2) S.F. = 2.08

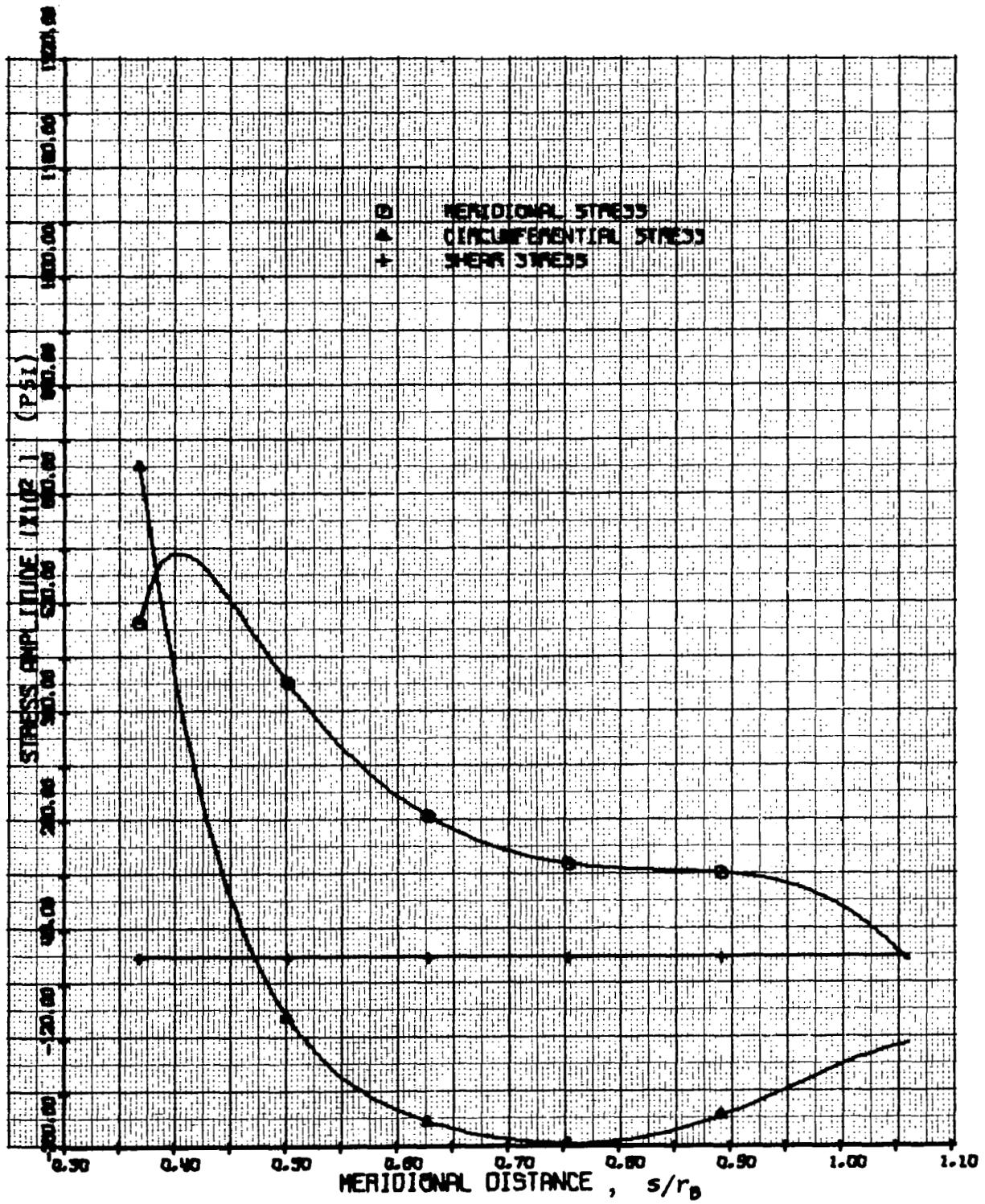

FIGURE 5. SHELL STRESS AMPLITUDES
140 DEG SANDWICH CONE, S.F. = 1.5
INNER FACE SHEET

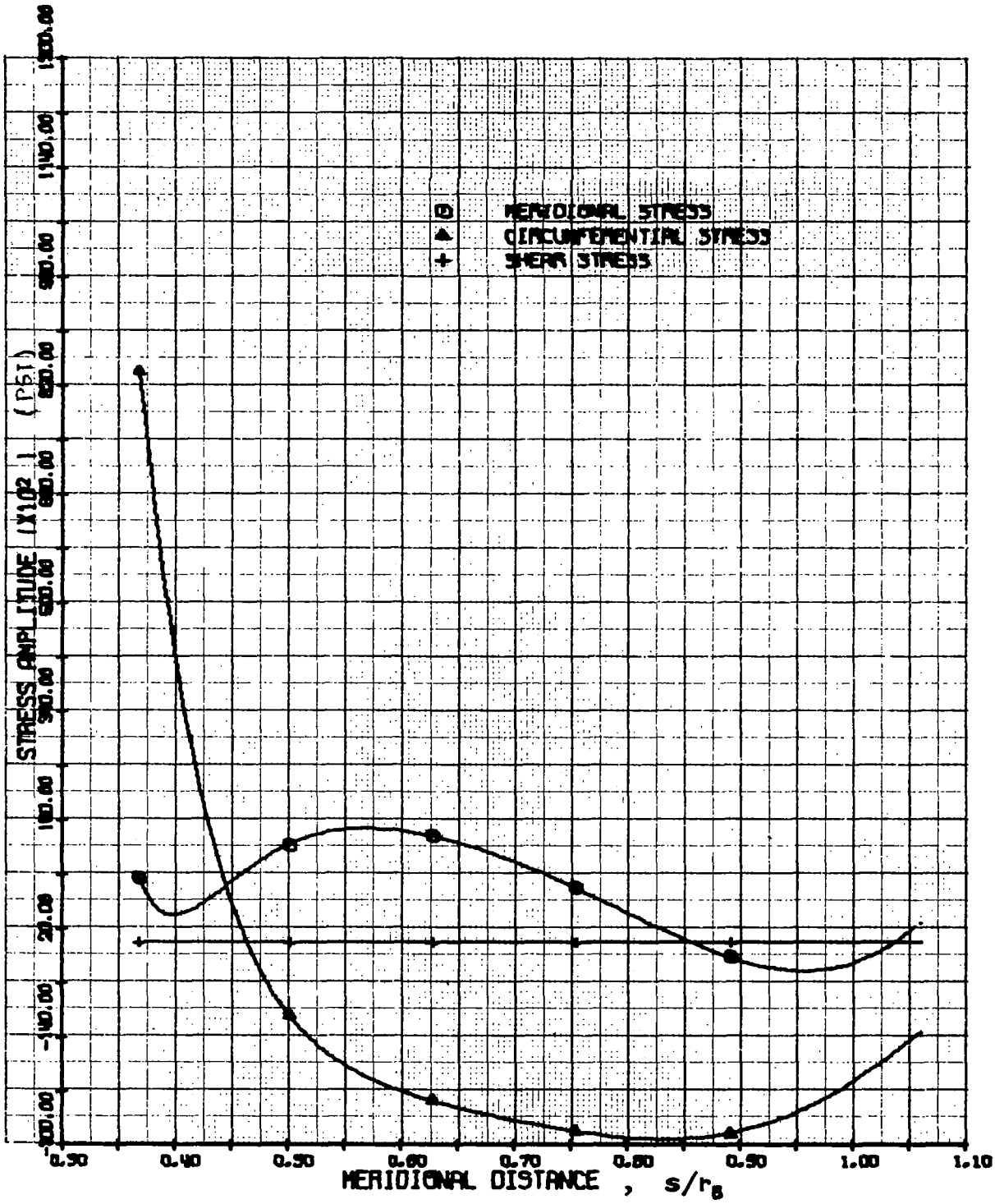

FIGURE 6. SHELL STRESS AMPLITUDES
140 DEG SANDWICH CONE, S.F. = 1.5
OUTER FACE SHEET

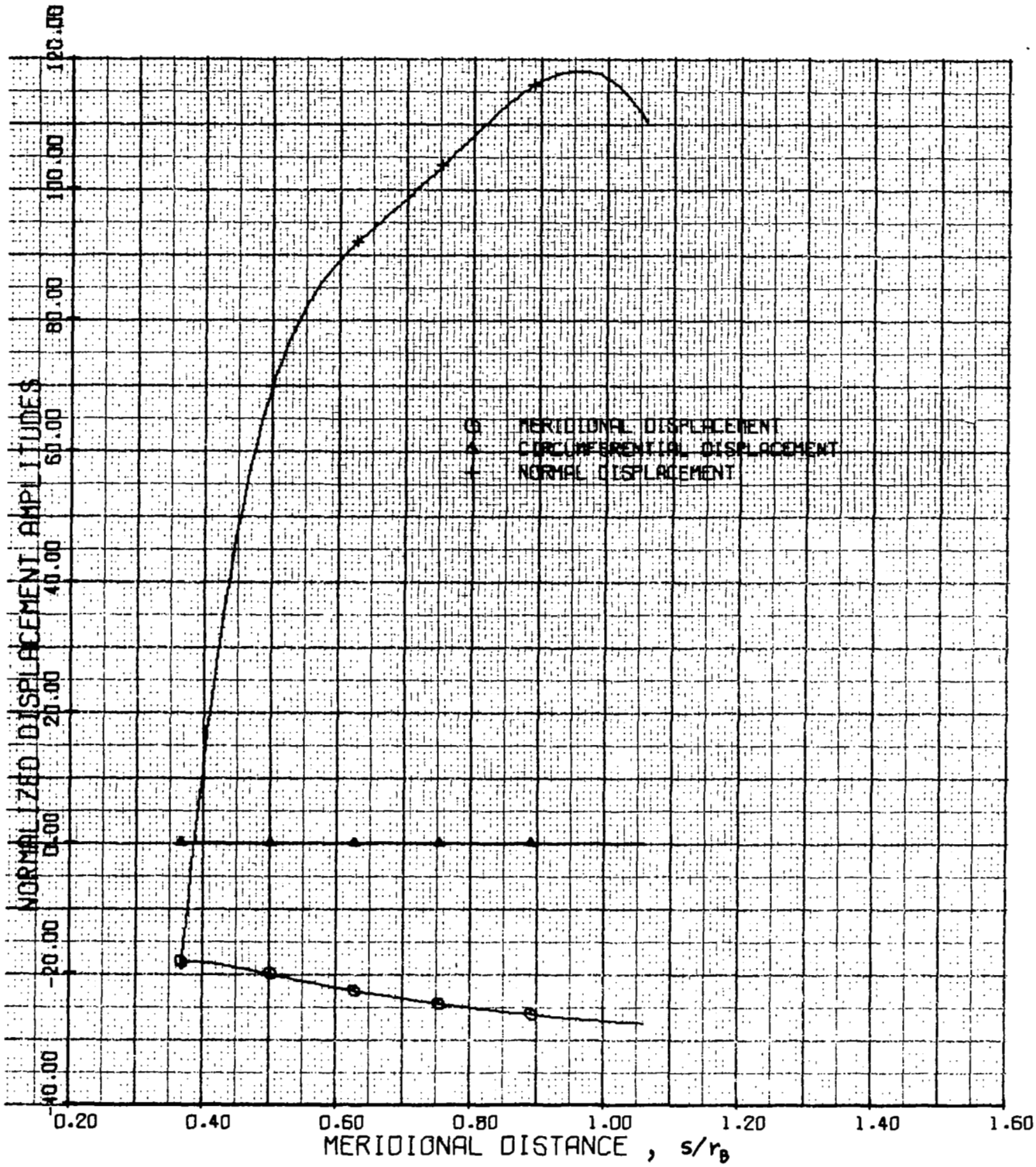

FIGURE 7. VIBRATION MODE DISPLACEMENTS
140 DEG SANDWICH CONE (N=0) FREQ = 30.1 CPS

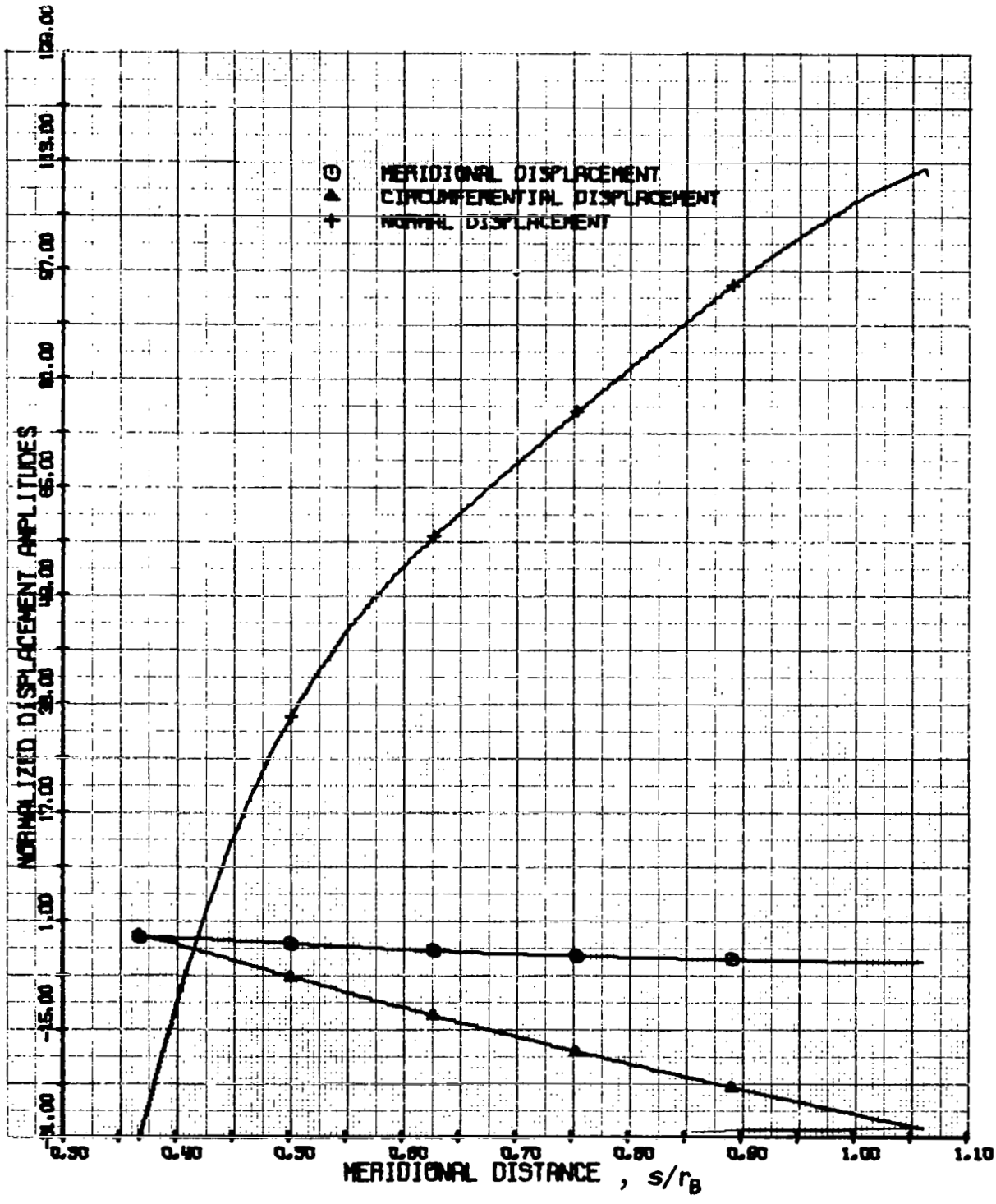

FIGURE 8. VIBRATION MODE DISPLACEMENTS
140 DEG SANDWICH CONE (N=1) FREQ = 15.4 CPS

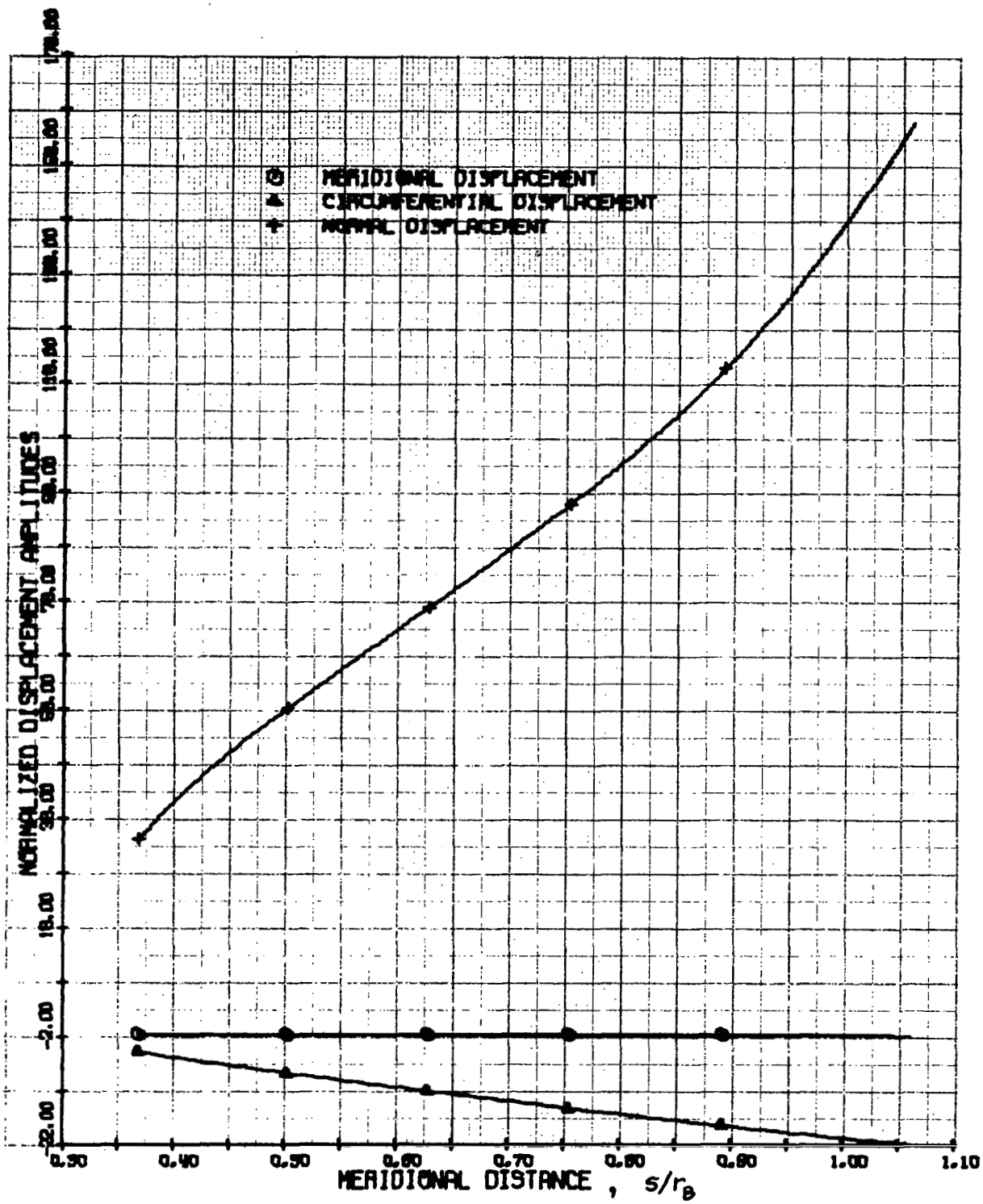

FIGURE 9. VIBRATION MODE DISPLACEMENTS
140 DEG SANDWICH CONE (N=2) FREQ = 13.1 CPS

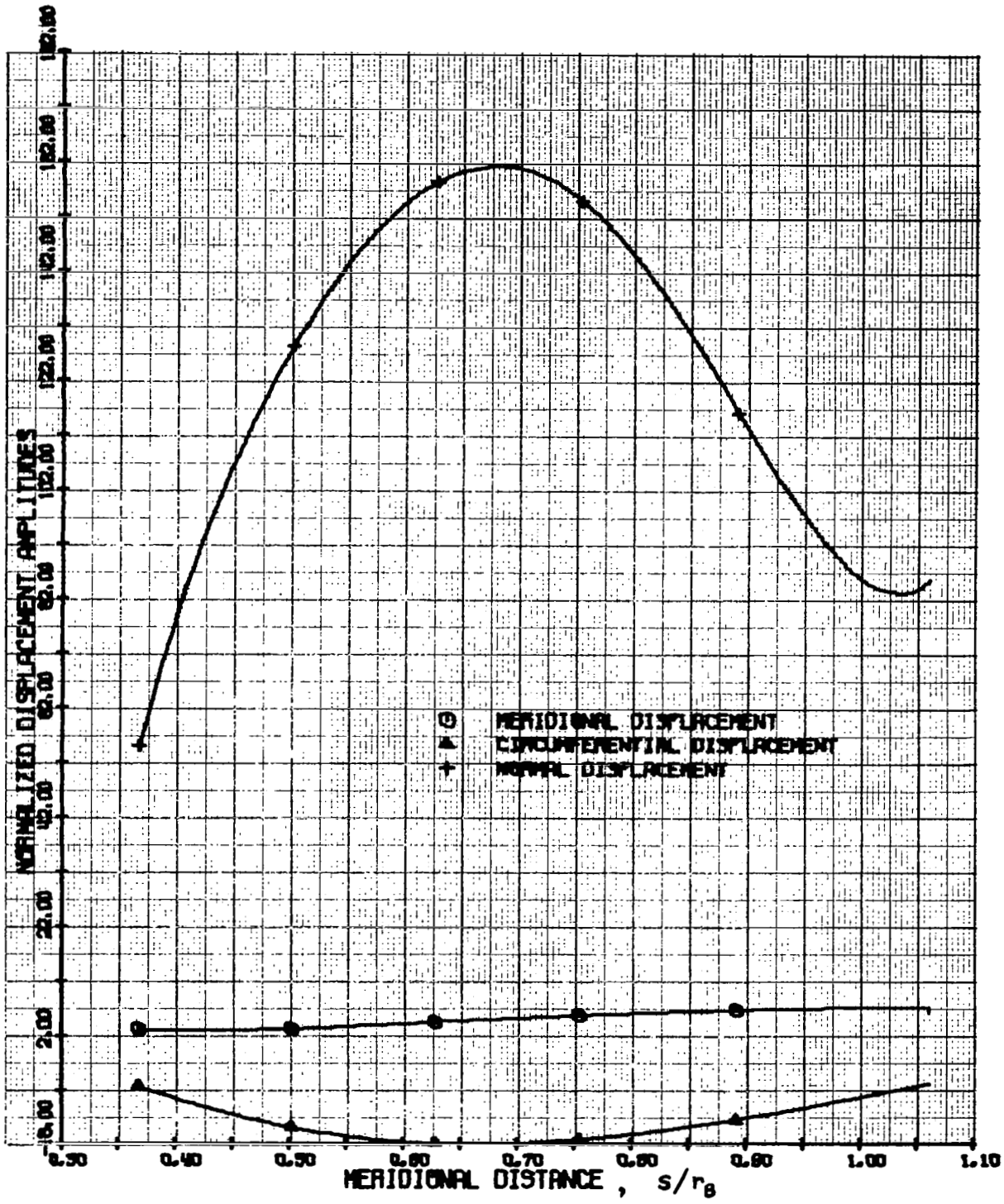

FIGURE 10. VIBRATION MODE DISPLACEMENTS
140 DEG SANDWICH CONE (N=3) FREQ = 34.5 CPS

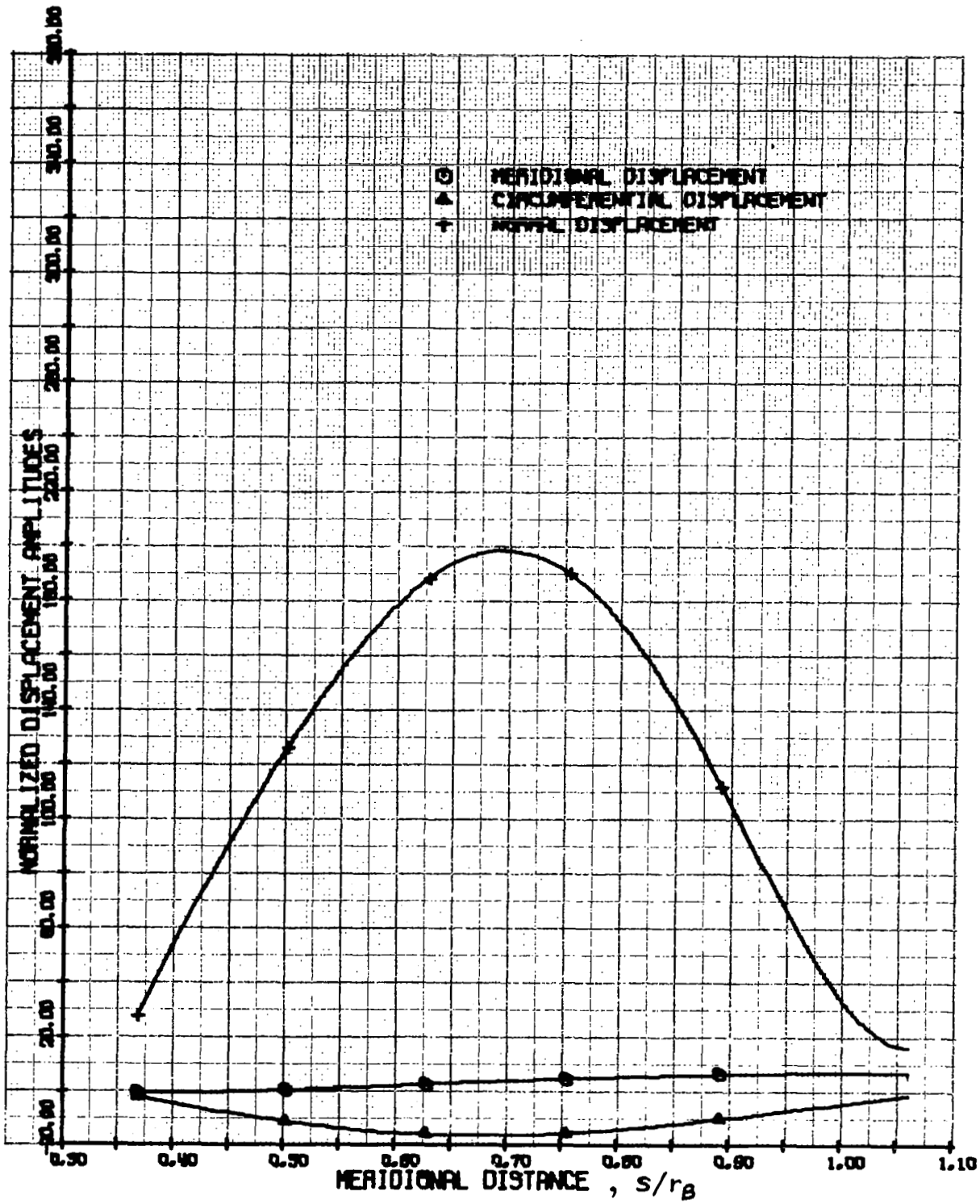

FIGURE 11. VIBRATION MODE DISPLACEMENTS
140 DEG SANDWICH CONE (N=4) FREQ = 42.8 CPS

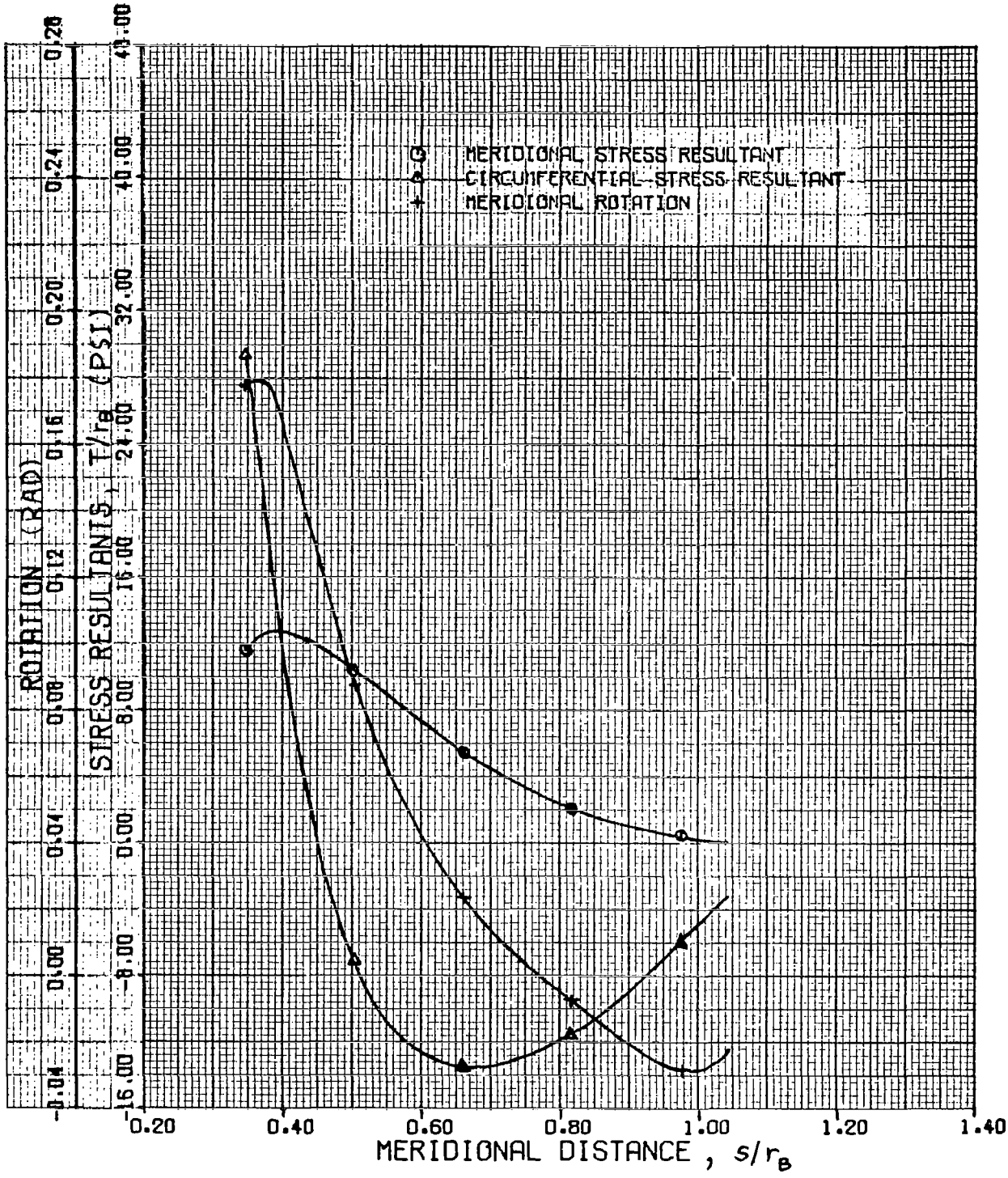

FIGURE 12. PREBUCKLING STRESS RESULTANTS AND ROTATION
60 DEGREE SANDWICH SPHERICAL DISH, S.F. = 2.25

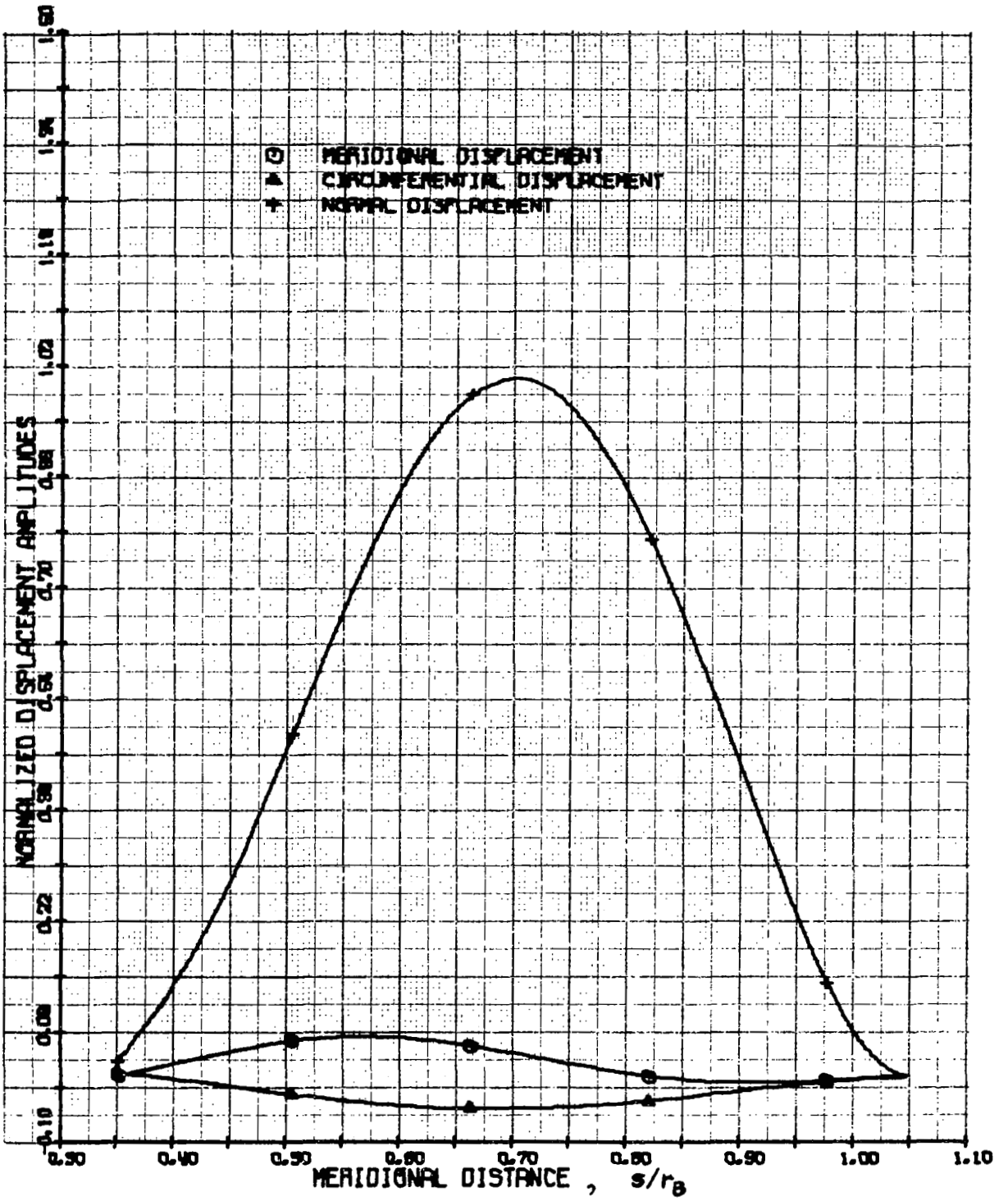

FIGURE 13. BUCKLING MODE DISPLACEMENTS
60 DEG SANDWICH SPHERICAL DISH (N=7) S.F. = 2.10

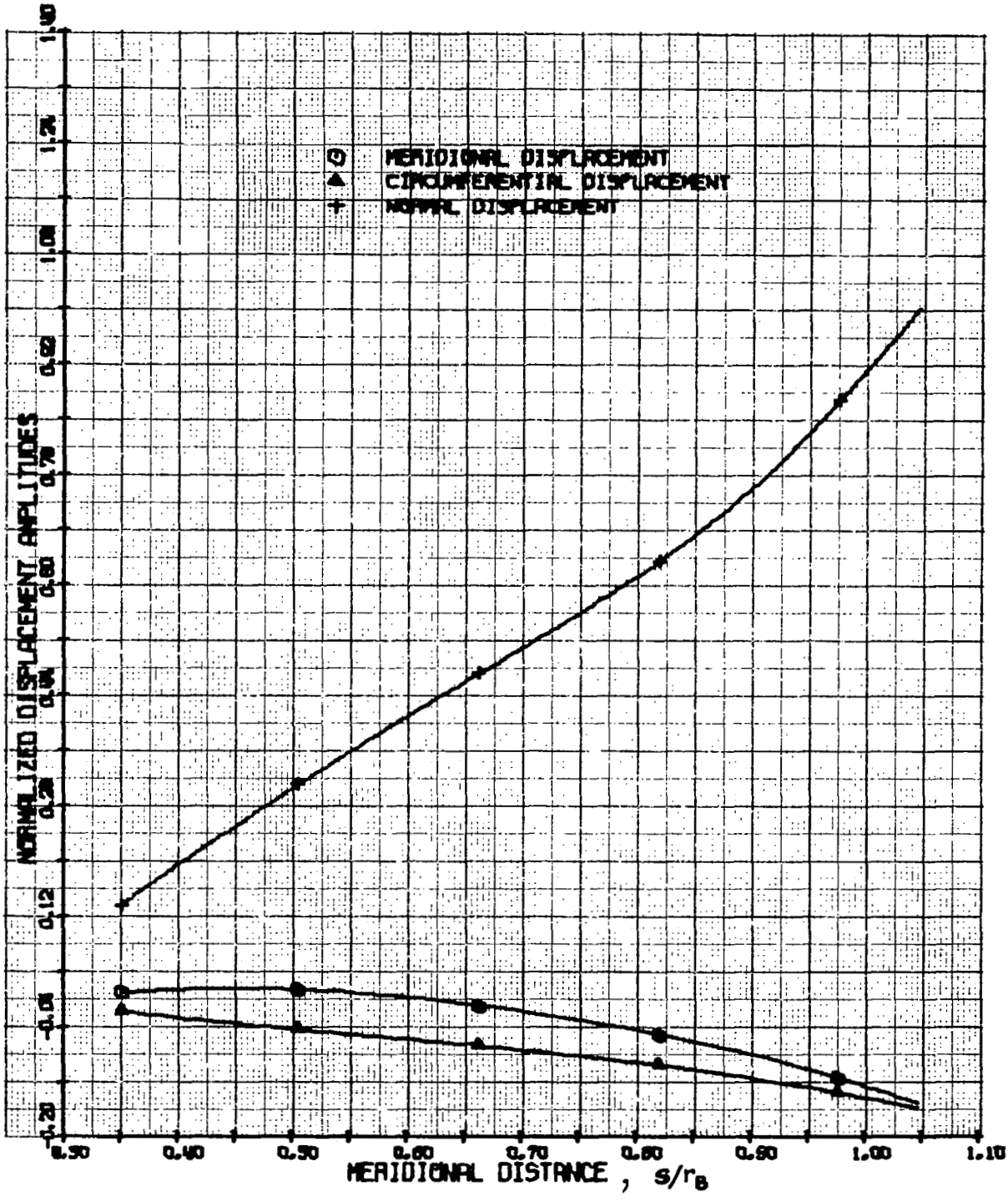

FIGURE 14. BUCKLING MODE DISPLACEMENTS
60 DEG SANDWICH SPHERICAL DISH (N=2) S.F. = 2.04

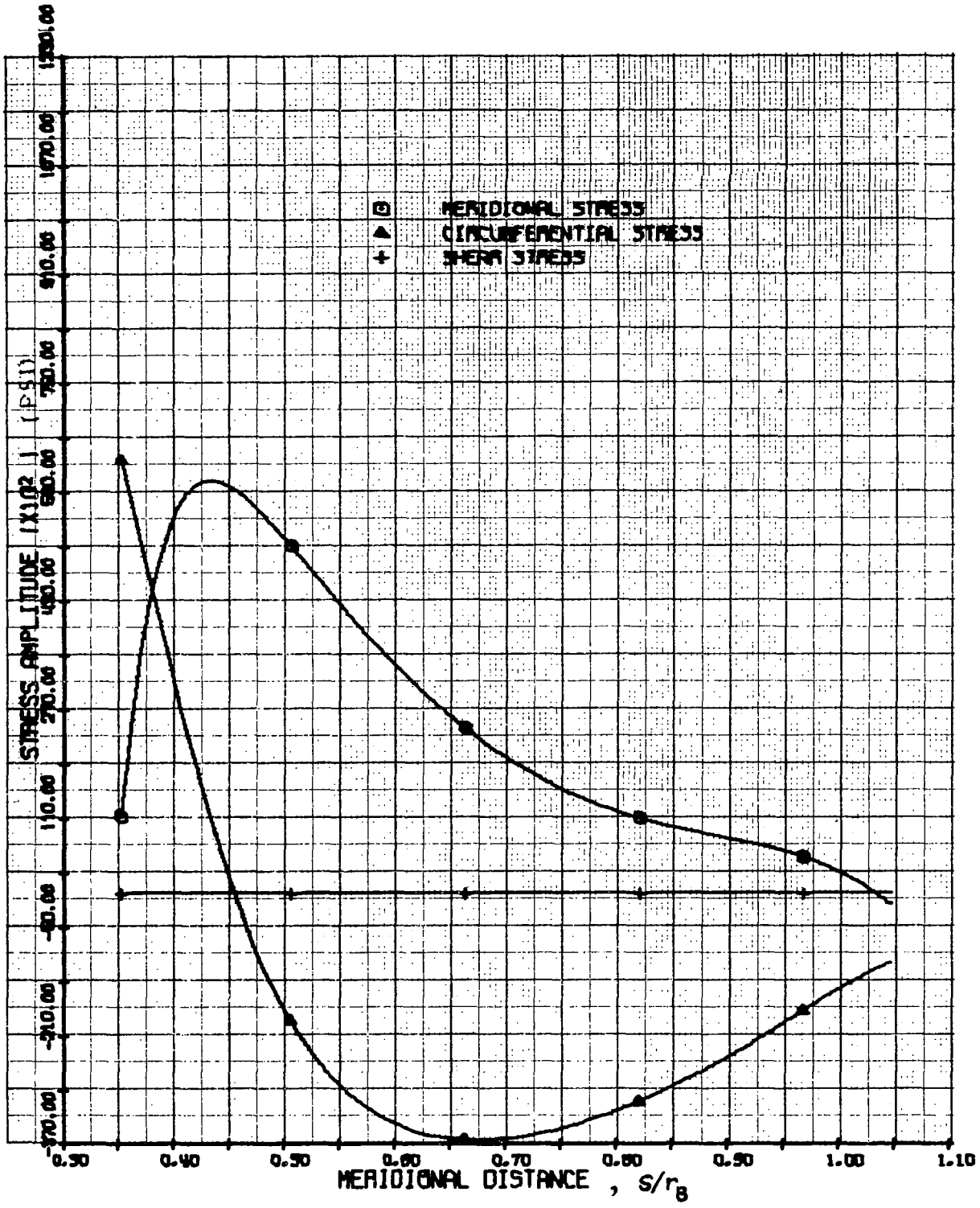

FIGURE 15. SHELL STRESS AMPLITUDES
60 DEG SANDWICH SPHERICAL DISH, S.F. = 1.5
INNER FACE SHEET

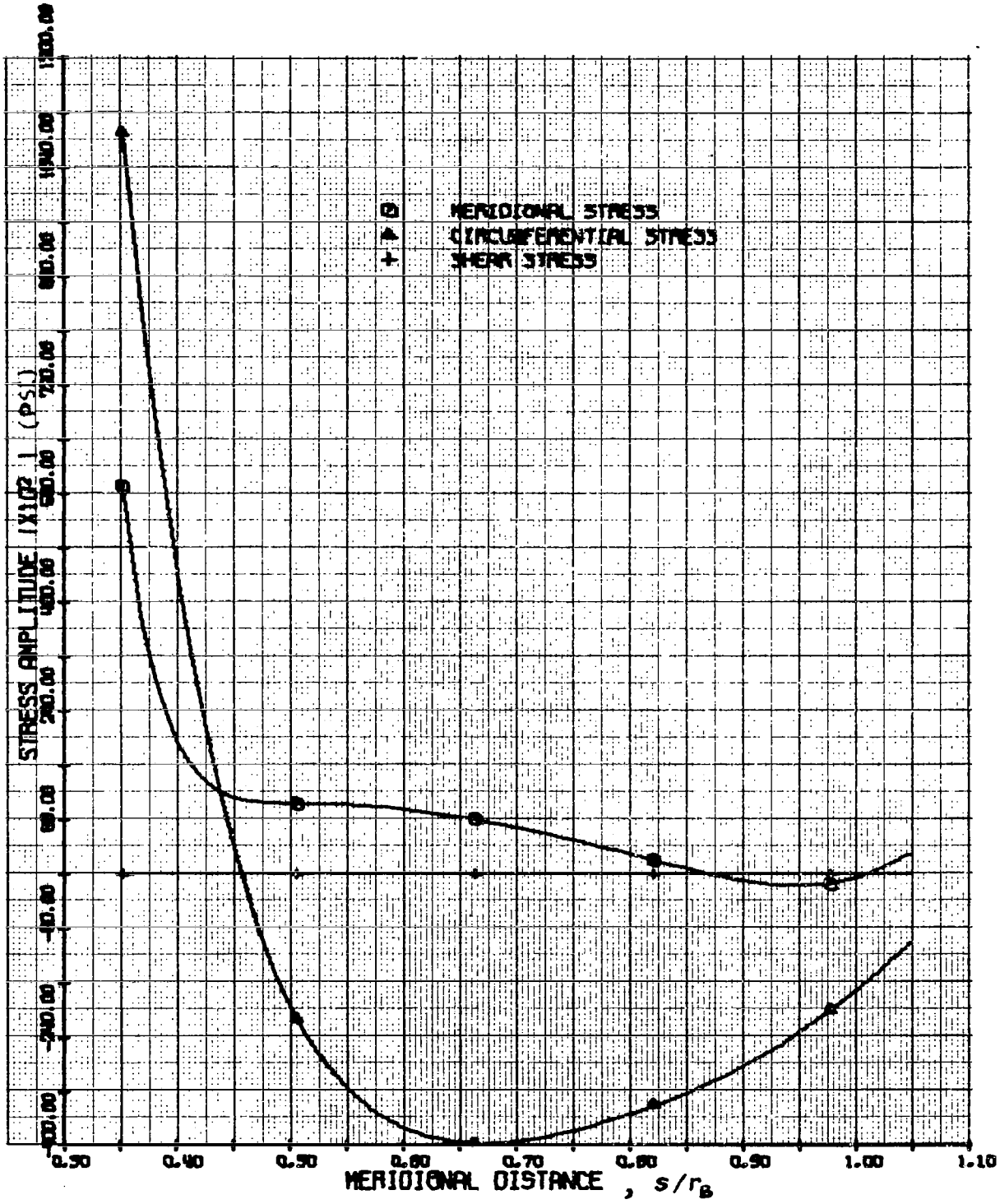

FIGURE 16. SHELL STRESS AMPLITUDES
60 DEG SANDWICH SPHERICAL DISH, S.F. = 1.5
OUTER FACE SHEET

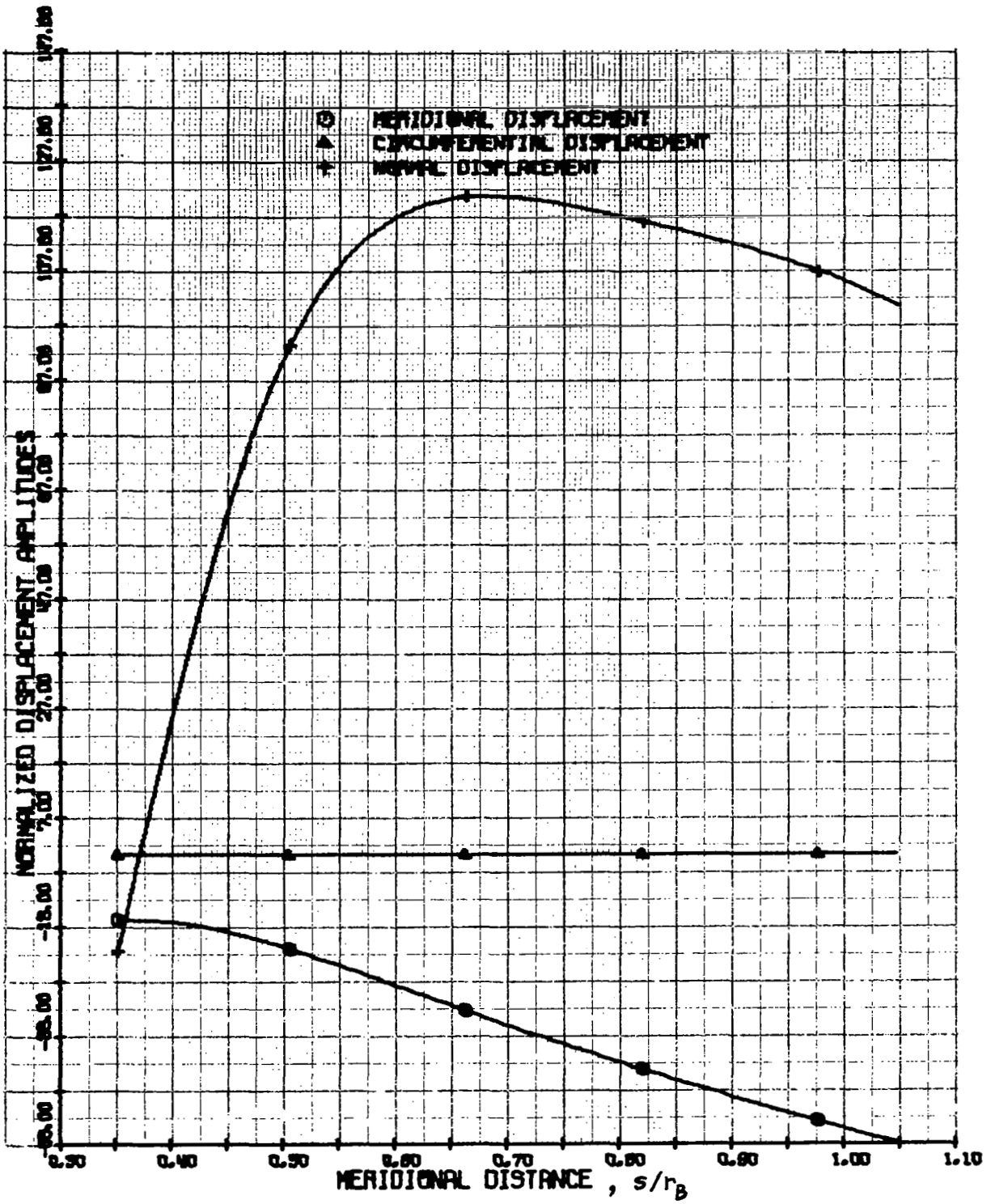

FIGURE 17. VIBRATION MODE DISPLACEMENTS
60 DEG SANDWICH SPHERICAL DISH (N=0) FREQ = 22.9 CPS

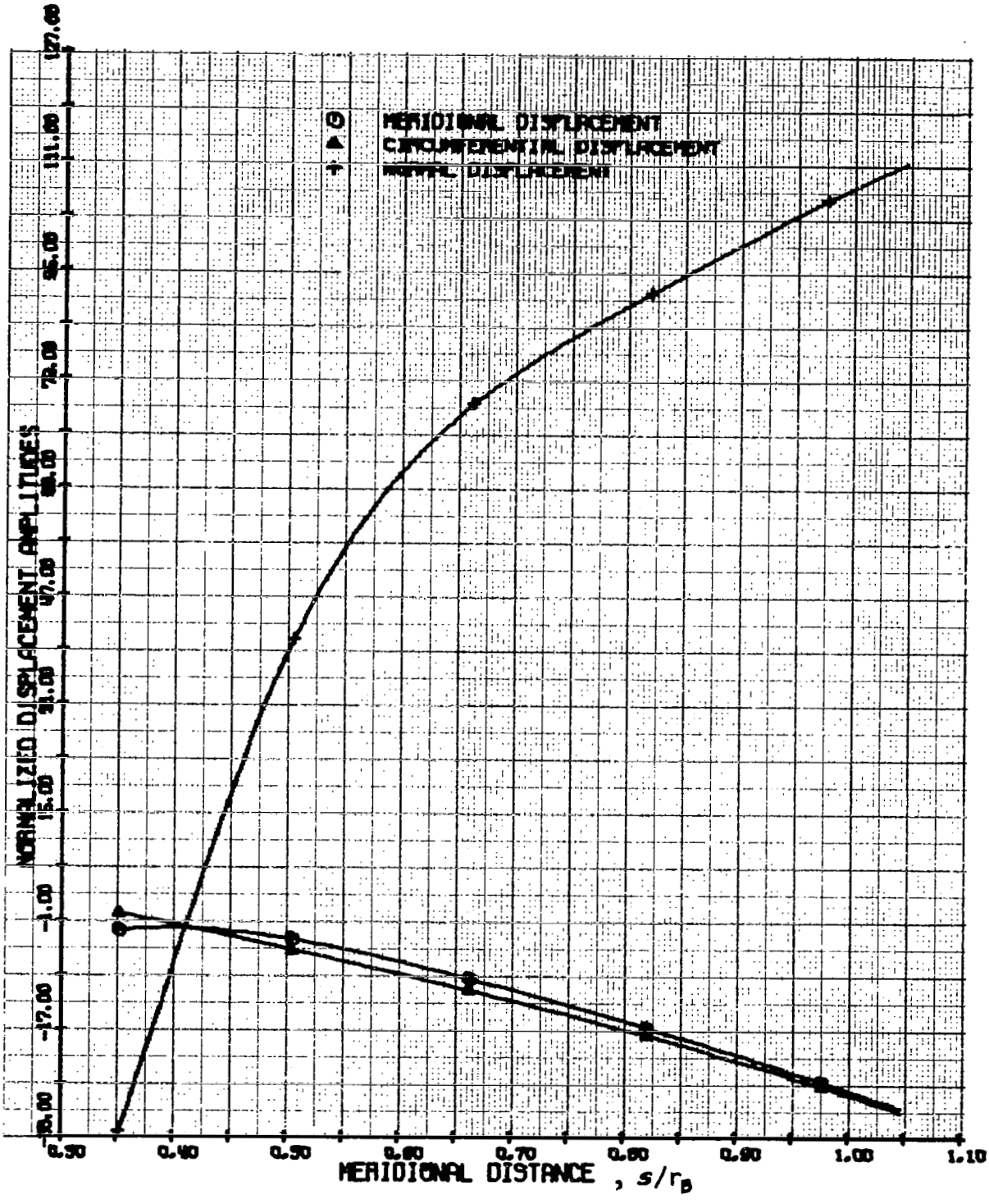

FIGURE 18. VIBRATION MODE DISPLACEMENTS
60 DEG SANDWICH SPHERICAL DISH (N=1) FREQ = 13.3 CPS

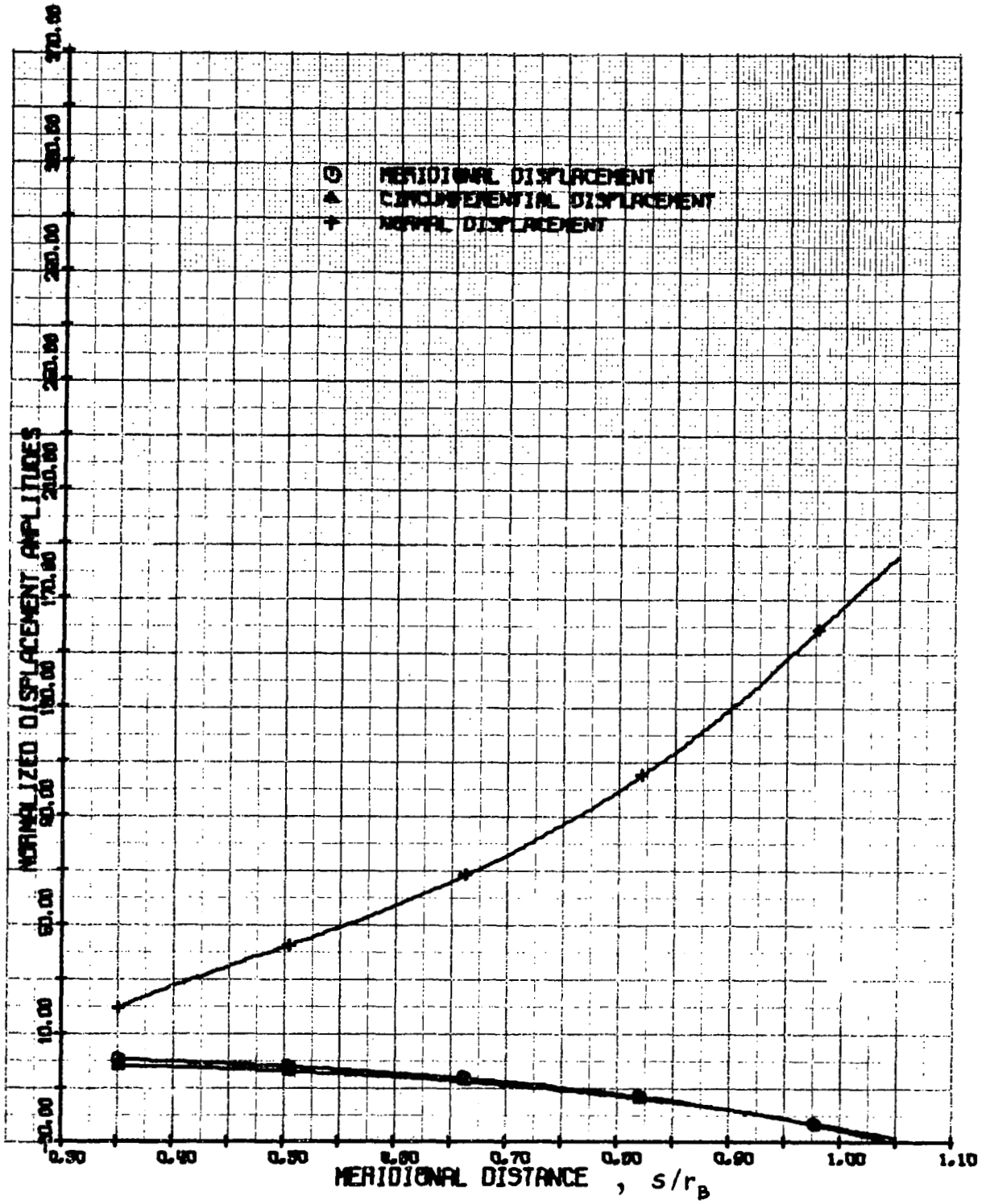

FIGURE 19. VIBRATION MODE DISPLACEMENTS
60 DEG SANDWICH SPHERICAL DISH (N=2) FREQ = 12.6 CPS

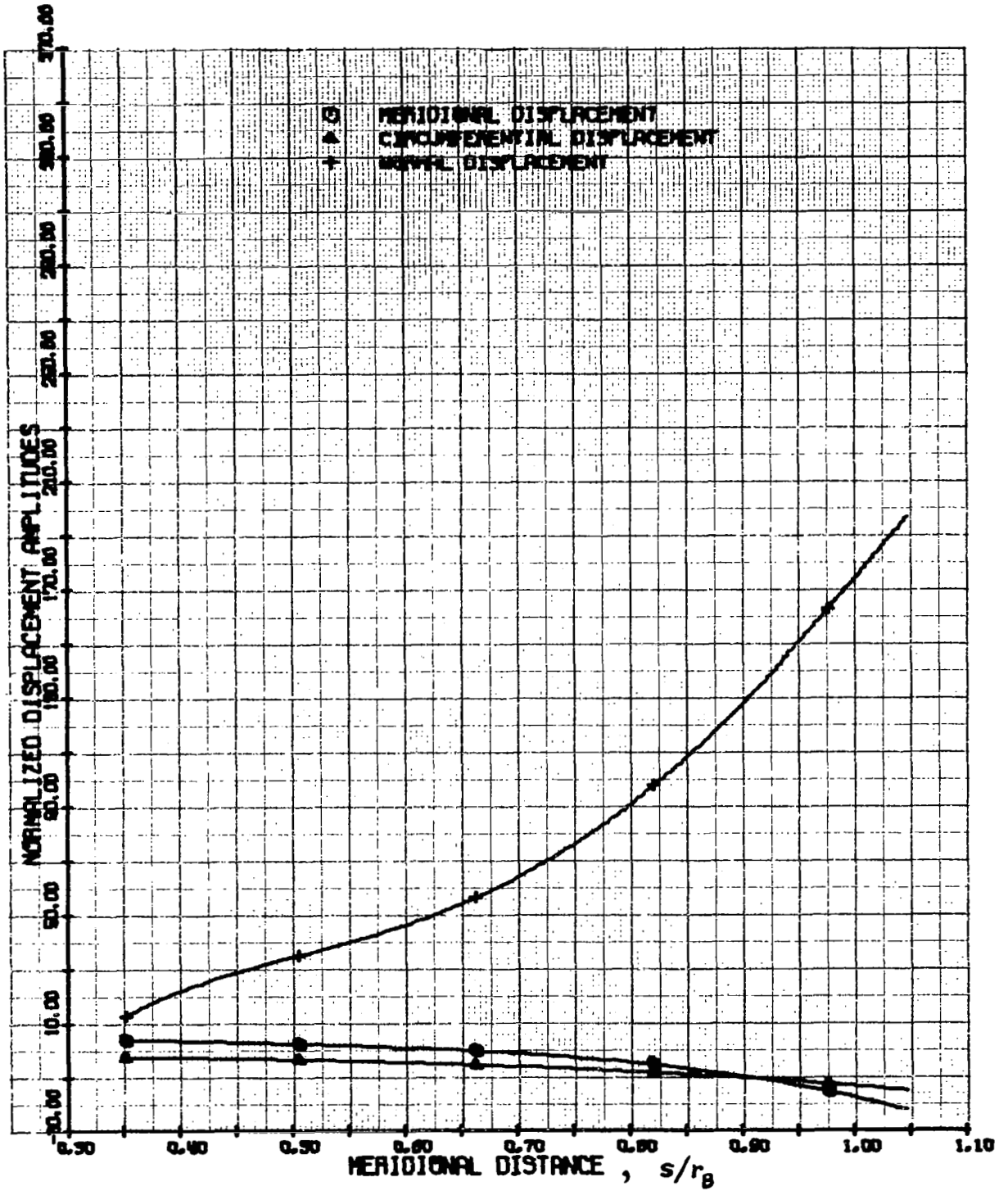

FIGURE 20. VIBRATION MODE DISPLACEMENTS
60 DEG SANDWICH SPHERICAL DISH (N=3) FREQ = 40.5 CPS

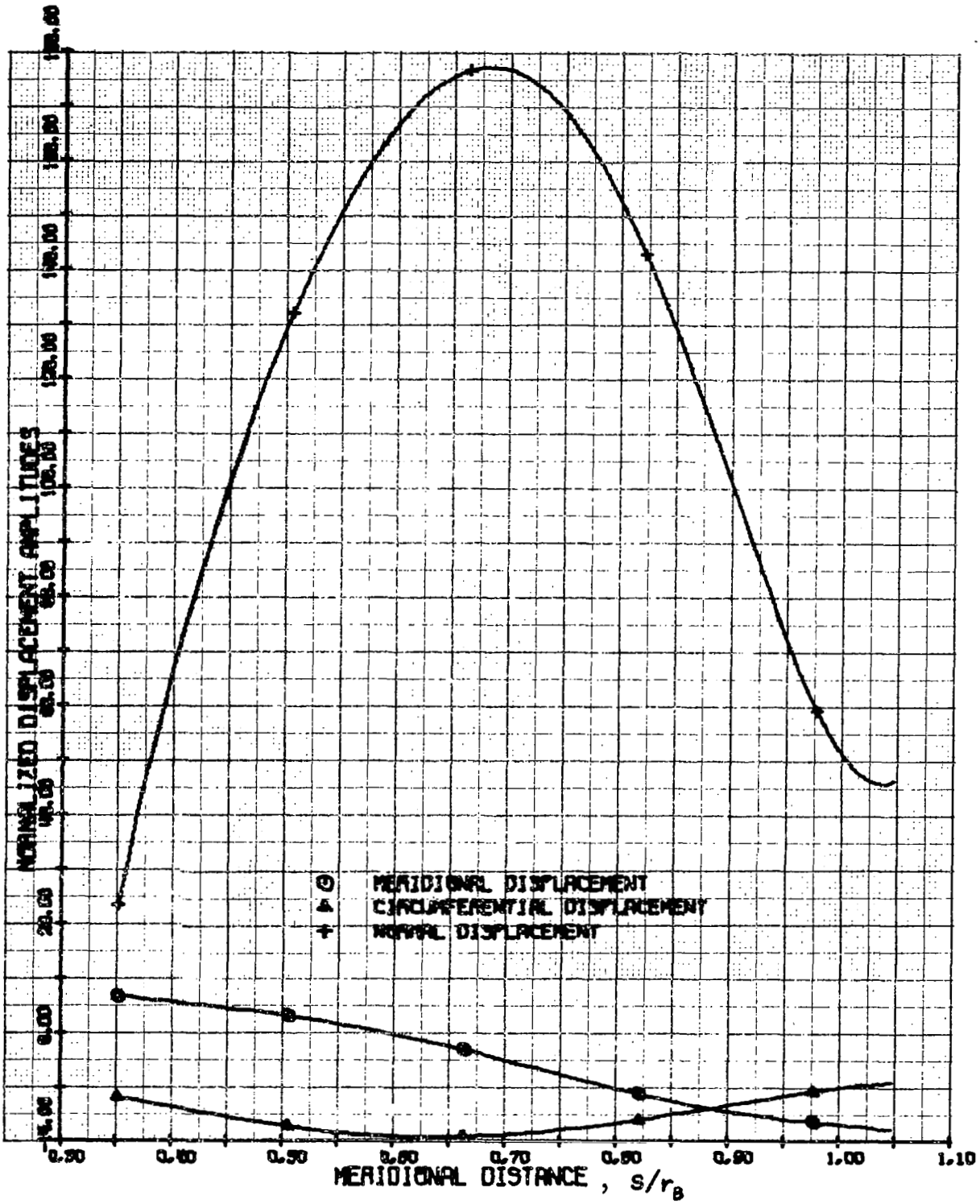

FIGURE 21. VIBRATION MODE DISPLACEMENTS
60 DEG SANDWICH SPHERICAL DISH (N=4) FREQ = 69.4 CPS

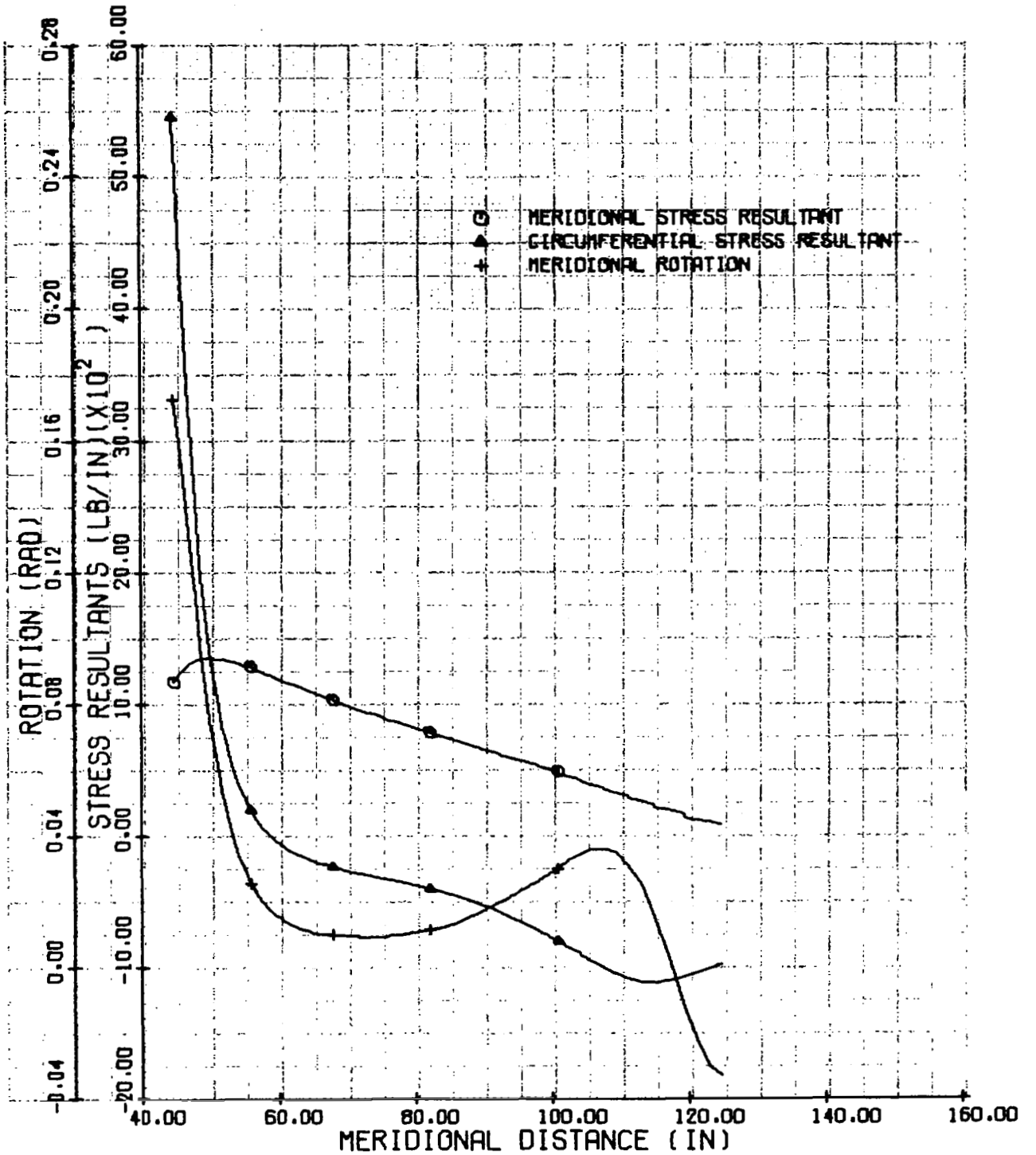

FIGURE 22 PREBUCKLING STRESS RESULTANTS AND ROTATION
OA.65 TENSION SHELL, S.F. = 2.25

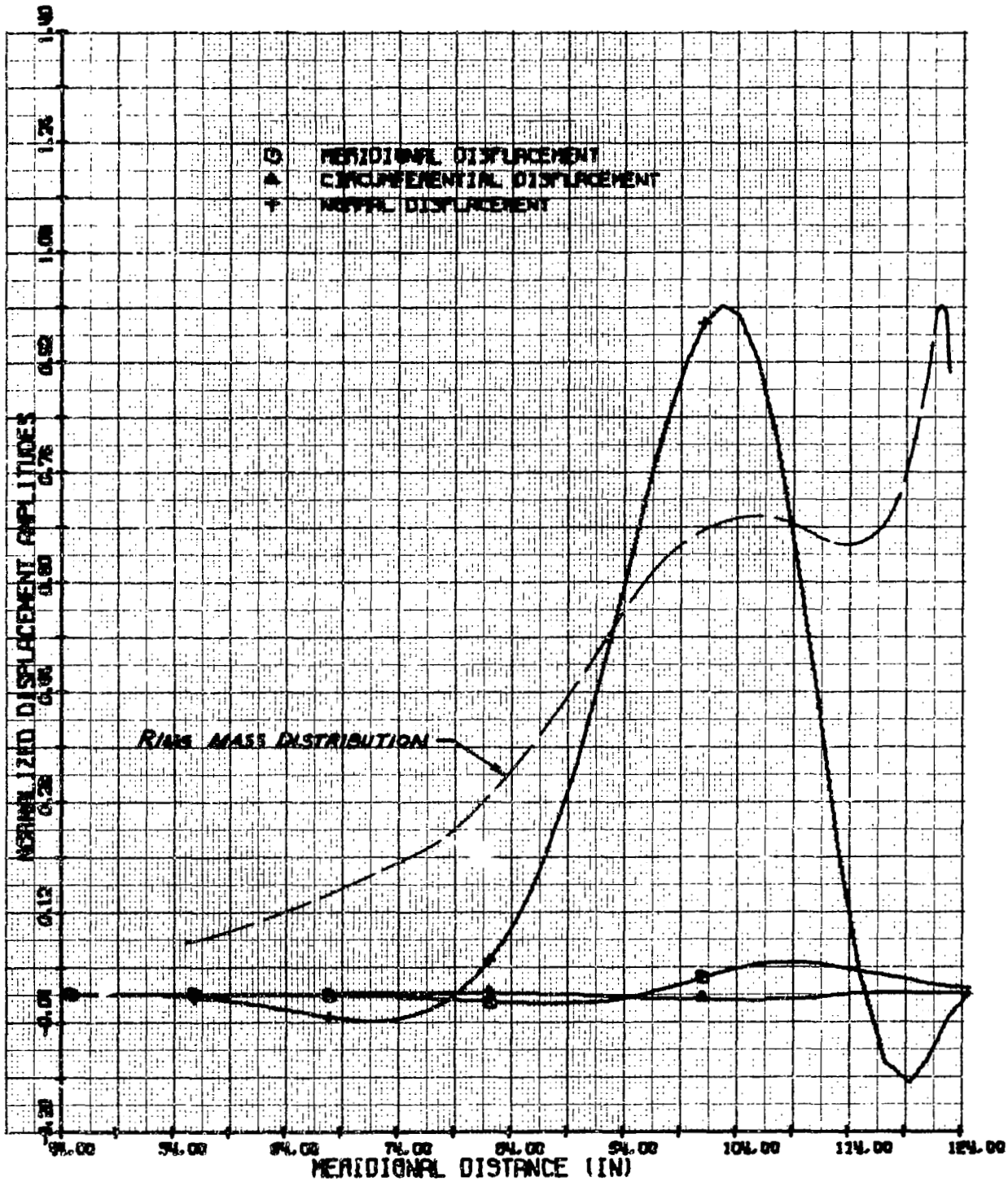

FIGURE 23. BUCLKING MODE DISPLACEMENTS
0A.65 TENSION SHELL (N=14) S.F. = 2.50

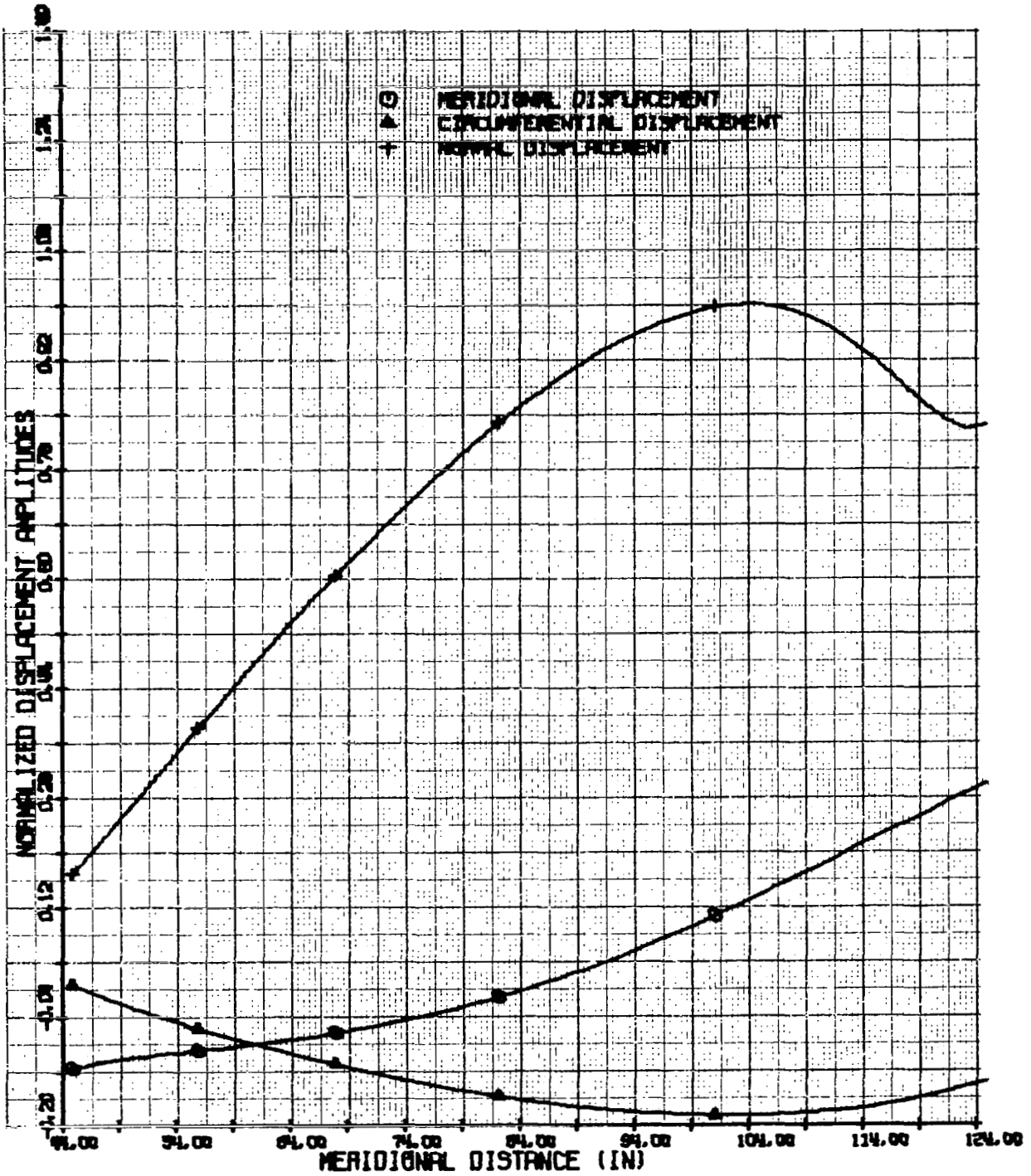

FIGURE 24. BUCKLING MODE DISPLACEMENTS
OA.65 TENSION SHELL (N=2) S.F. = 2.21

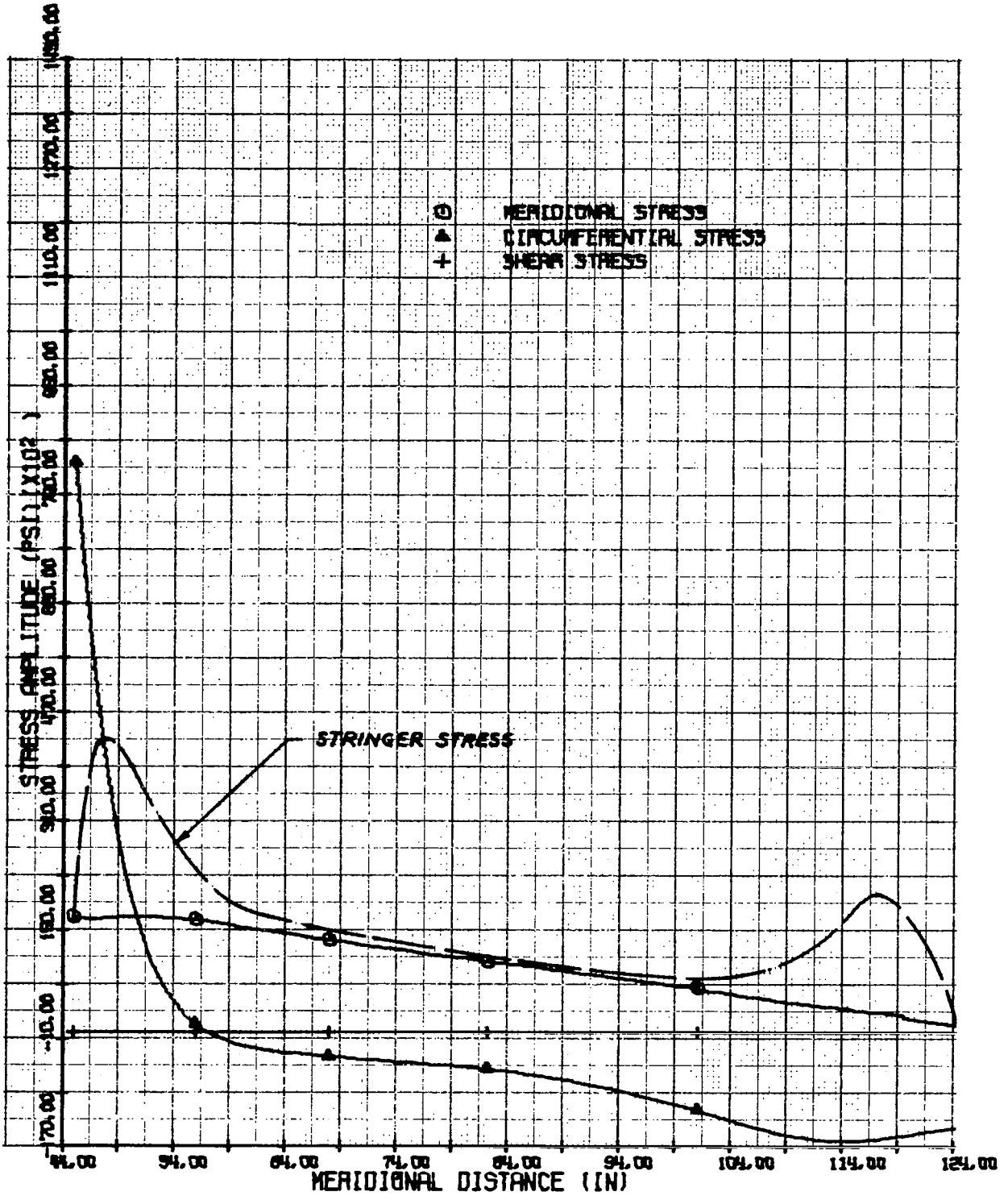

FIGURE 25. SHELL STRESS AMPLITUDES
OA.65 TENSION SHELL, S.F. = 1.5
INNER FACE

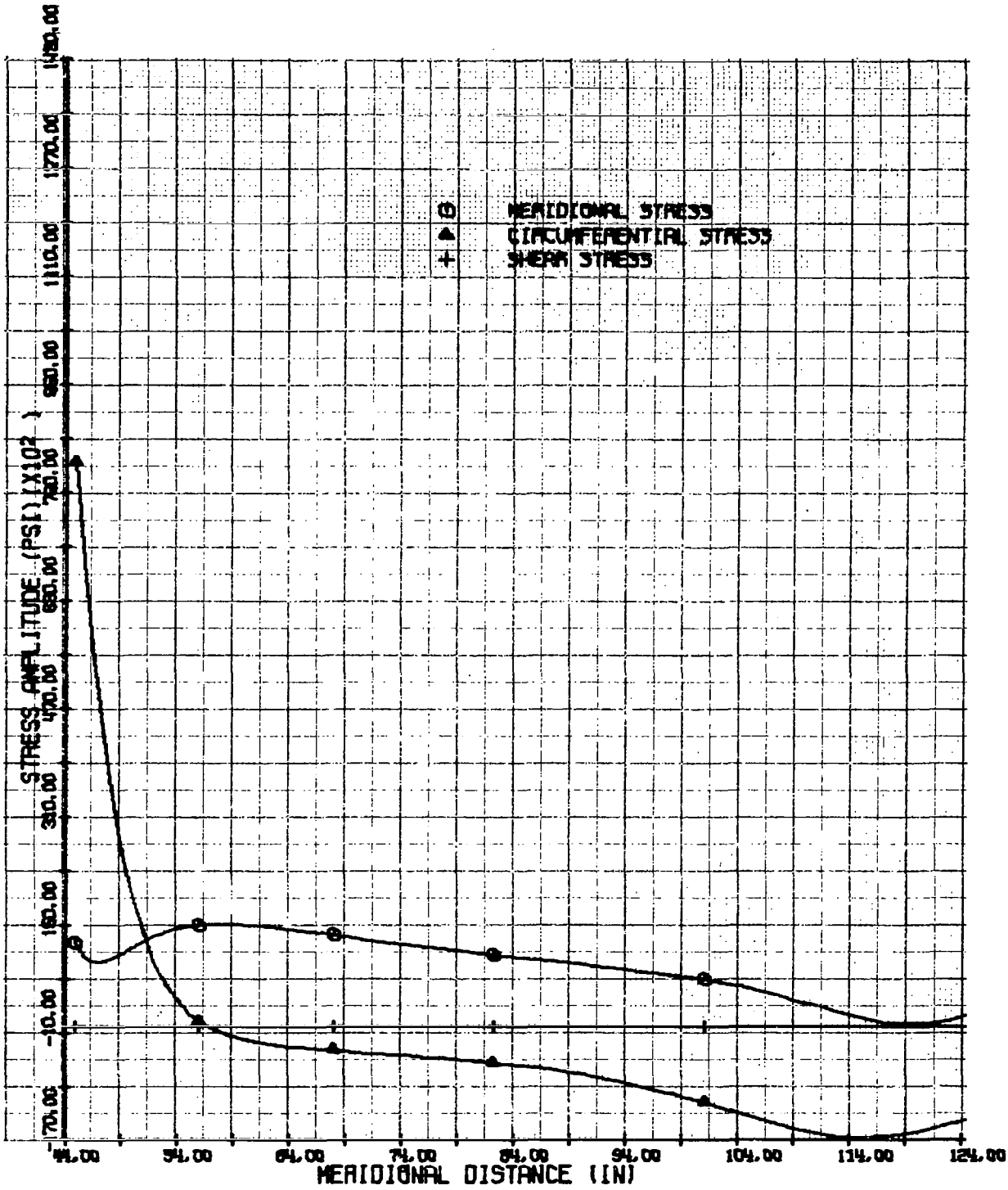

FIGURE 26. SHELL STRESS AMPLITUDES
0A.65 TENSION SHELL, S.F. = 1.5
OUTER FACE

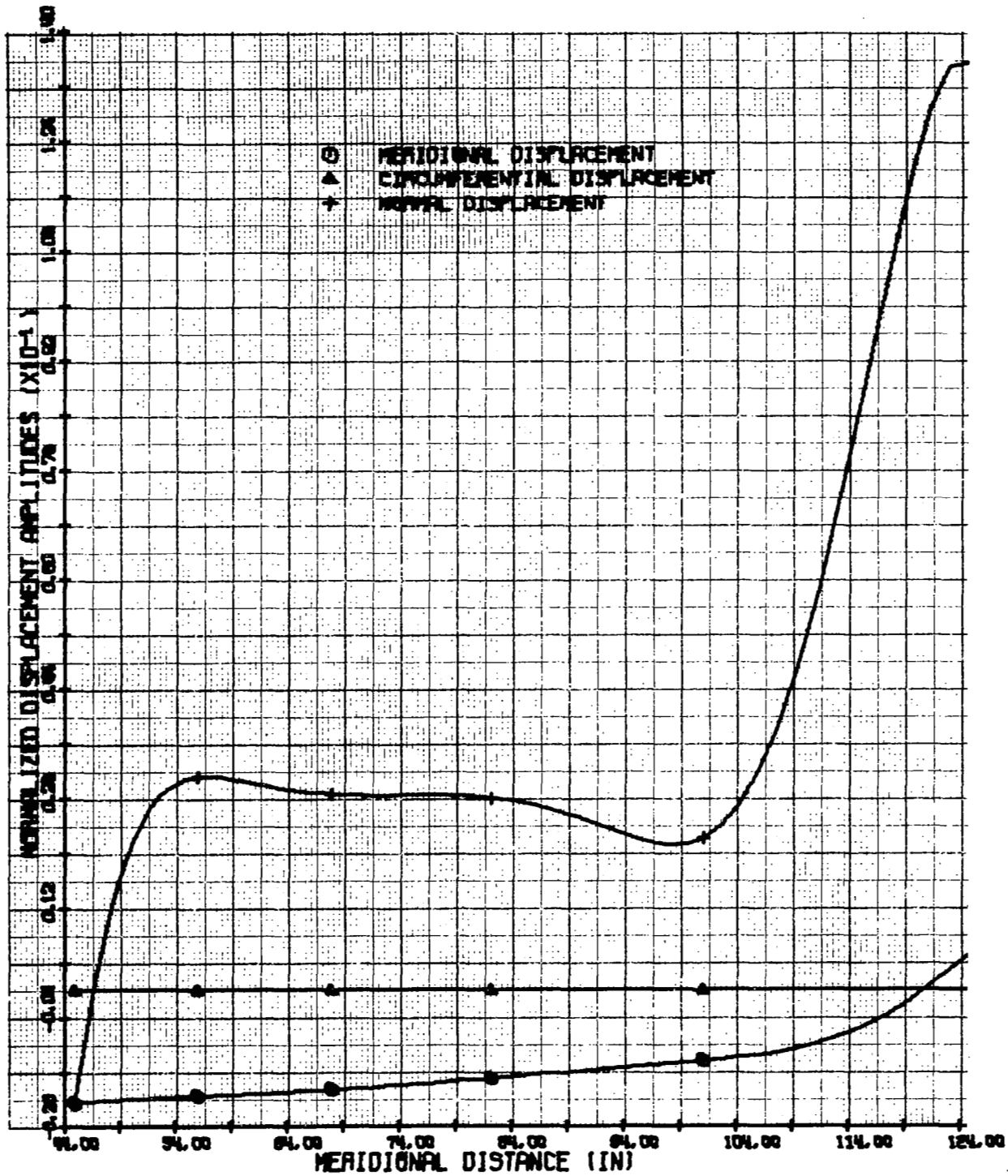

FIGURE 27. VIBRATION MODE DISPLACEMENTS
OA.65 TENSION SHELL (N=0) FREQ = 27.8 CPS

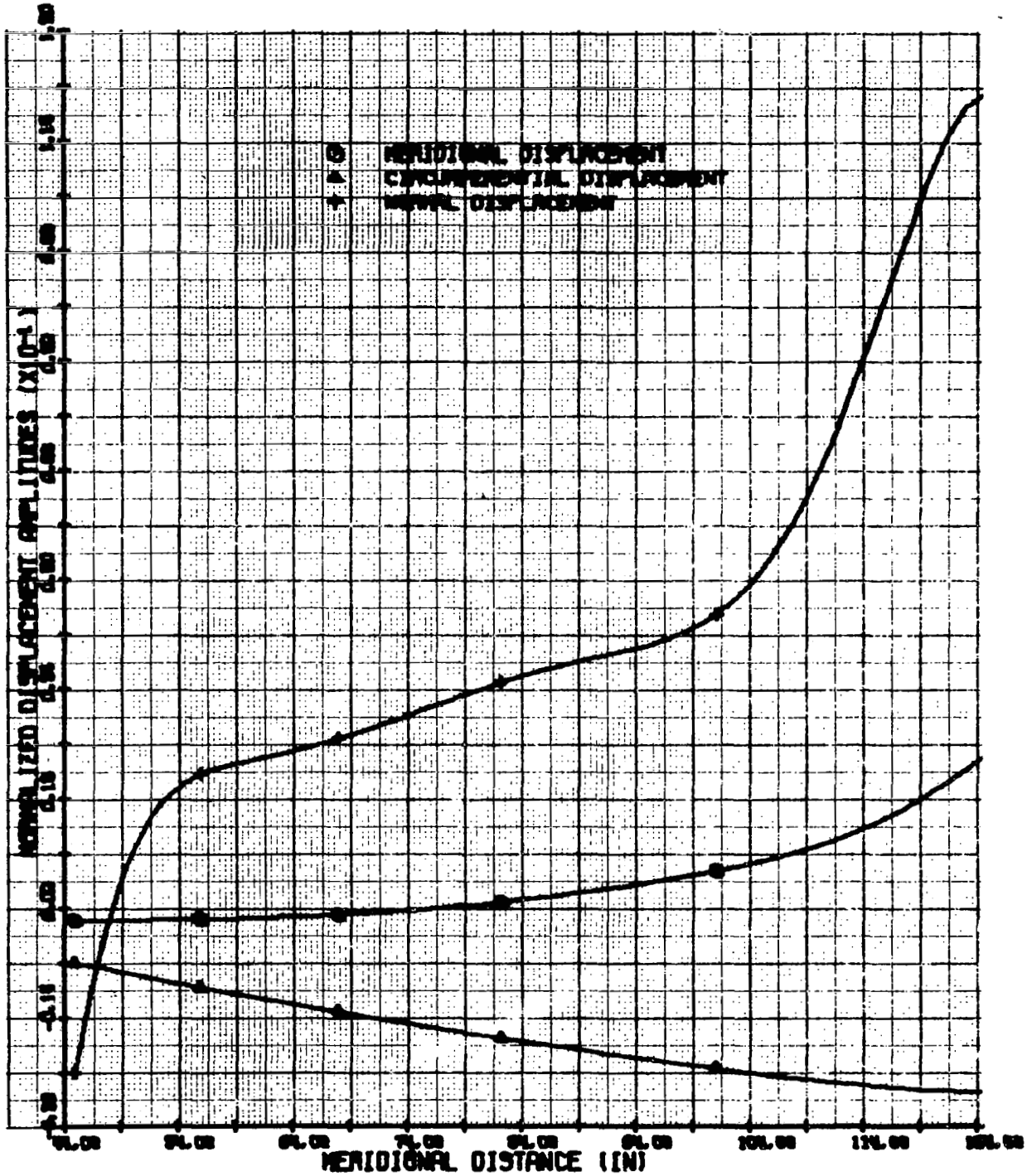

FIGURE 28. VIBRATION MODE DISPLACEMENTS
OA.65 TENSION SHELL (N=1) FREQ = 21.3 CPS

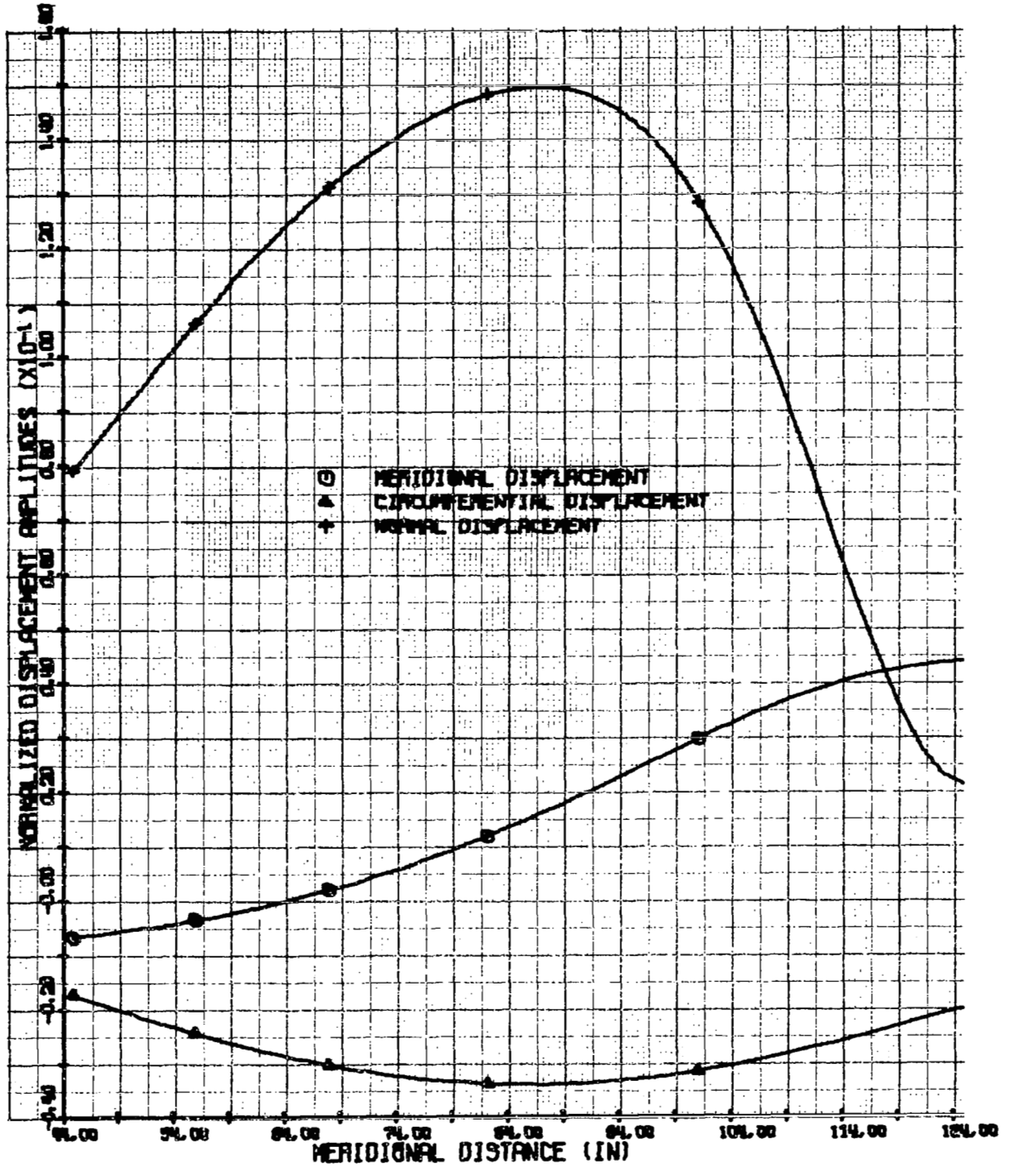

FIGURE 29. VIBRATION MODE DISPLACEMENTS
OA.65 TENSION SHELL (N=2) FREQ = 8.53 CPS

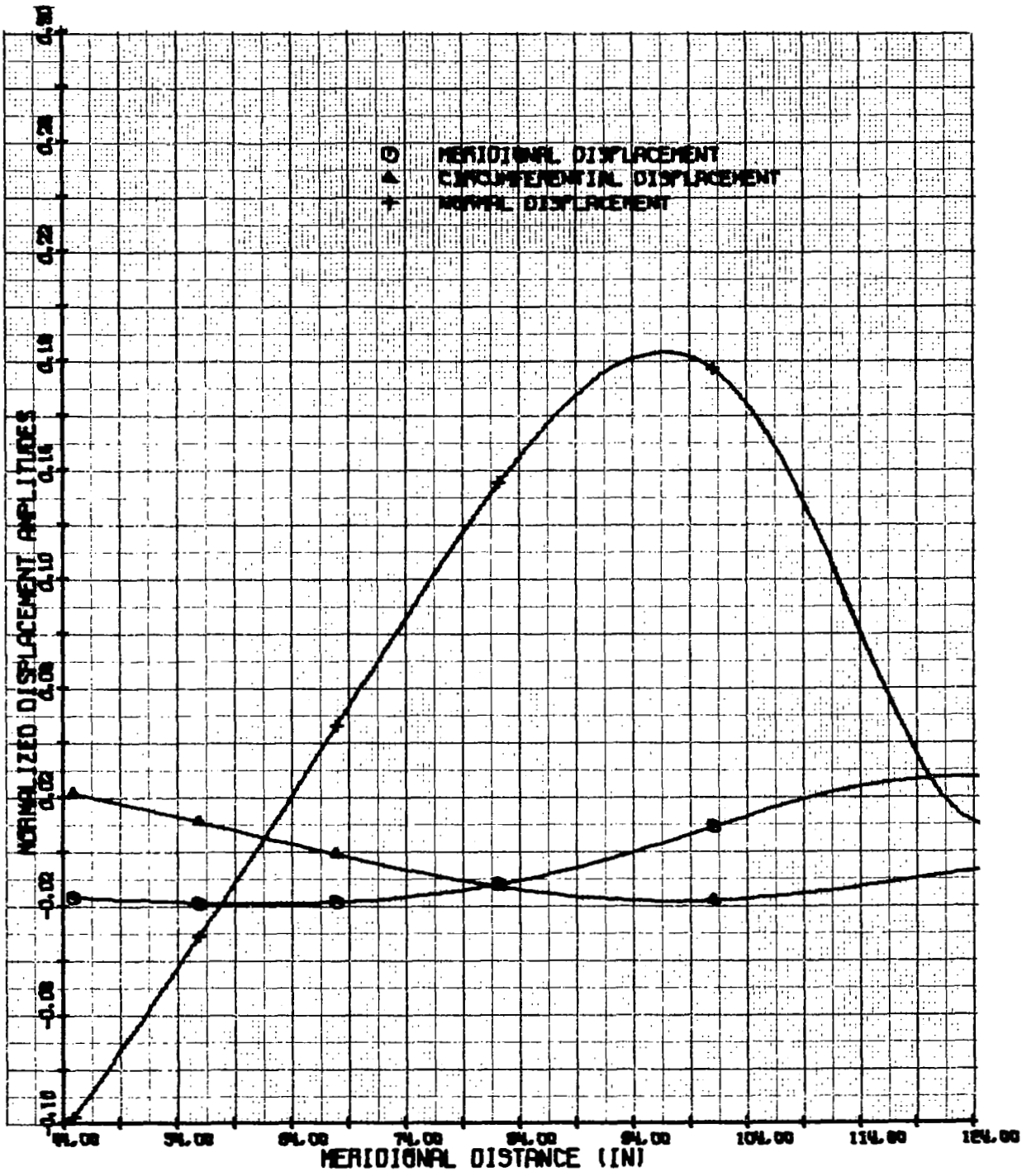

FIGURE 30. VIBRATION MODE DISPLACEMENTS
OA.65 TENSION SHELL (N=3) FREQ = 15.8 CPS

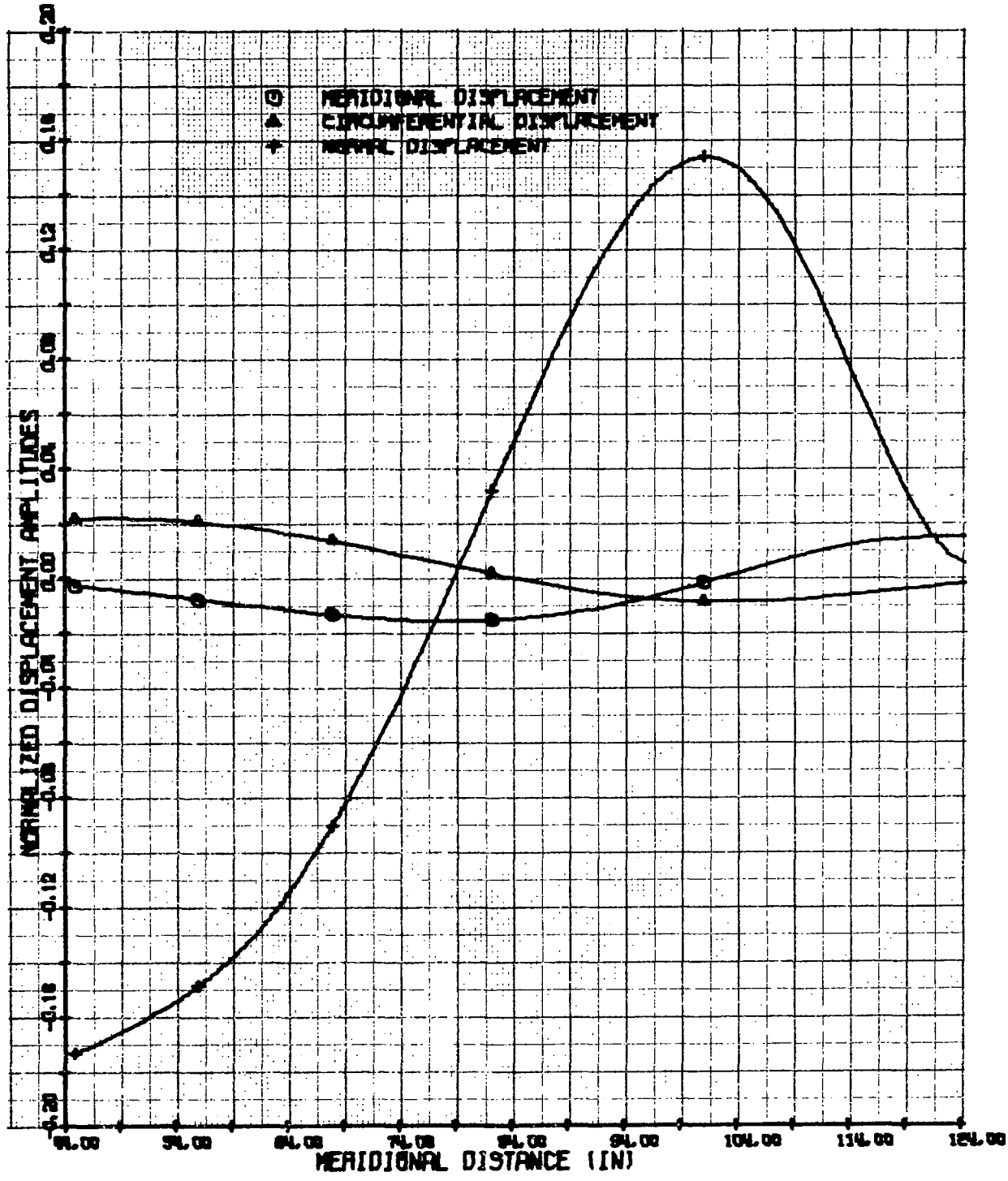

FIGURE 31. VIBRATION MODE DISPLACEMENTS
OA.65 TENSION SHELL (N=4) FREQ = 21.3 CPS

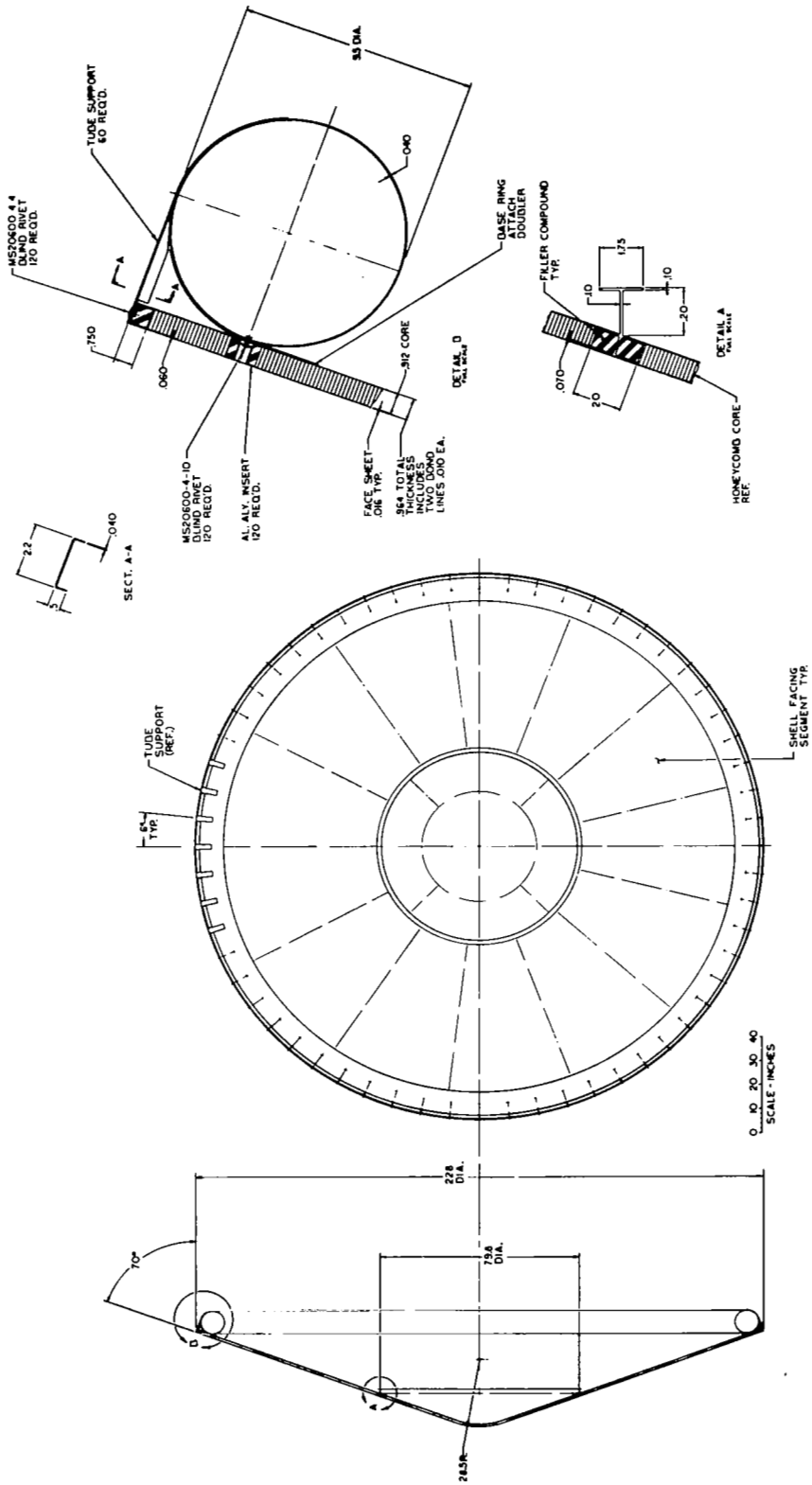

FIGURE 32. HONEYCOMB SANDWICH CONE

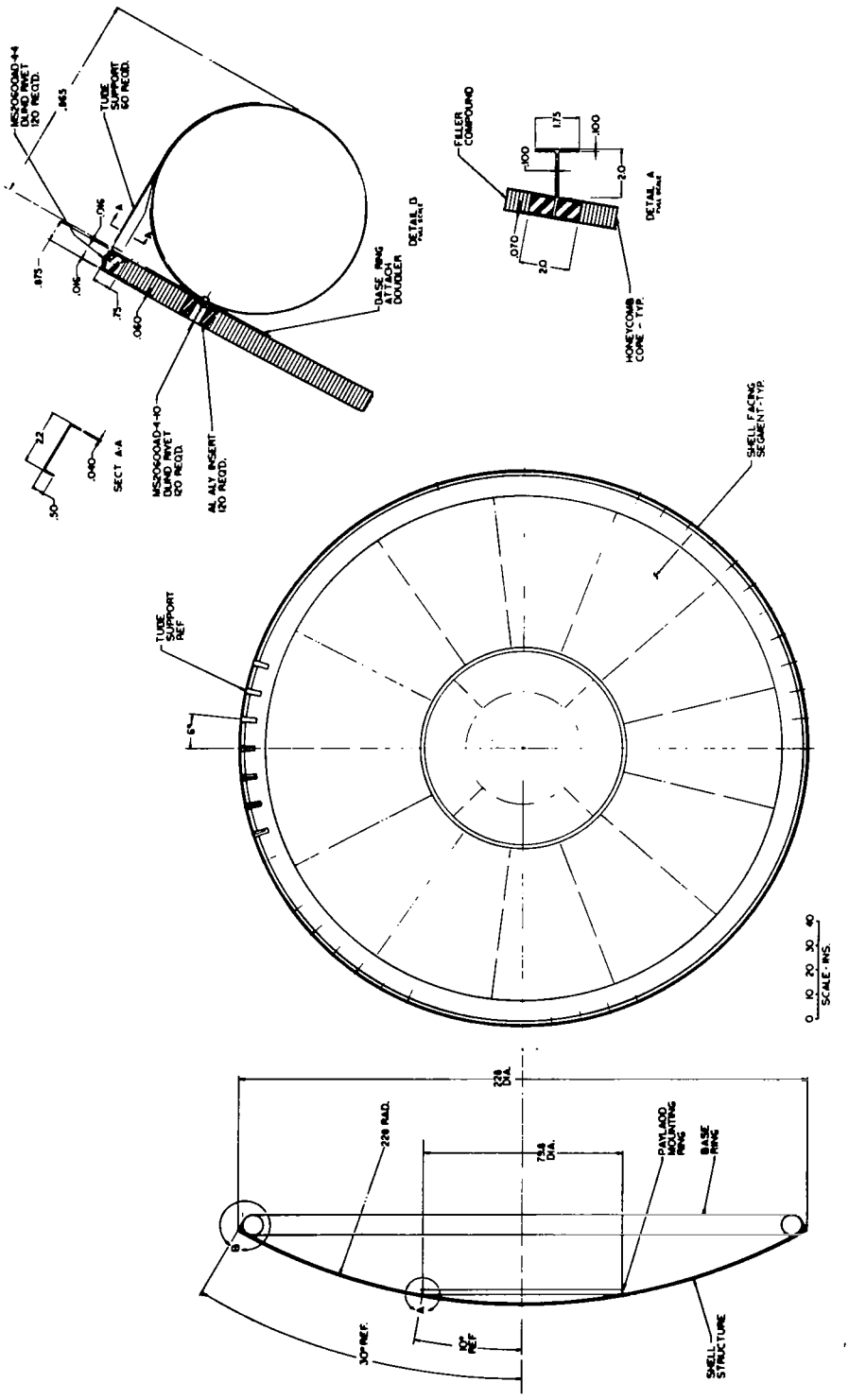

FIGURE 33. HONEYCOMB SANDWICH SPHERICAL DISH

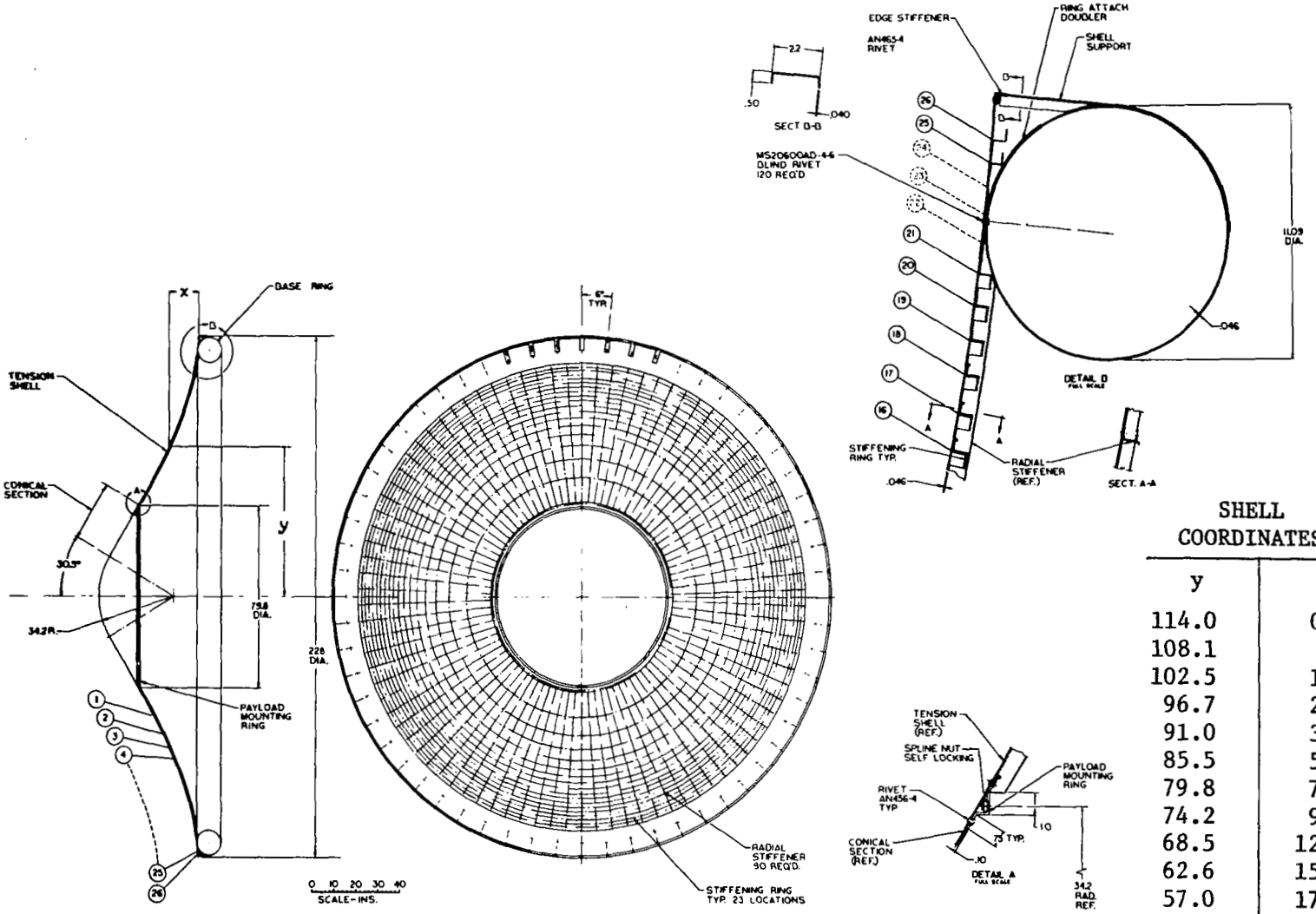

FIGURE 34. OA.65 TENSION SHELL

SHELL COORDINATES

y	x
114.0	0.0
108.1	.57
102.5	1.368
96.7	2.51
91.0	3.99
85.5	5.70
79.8	7.64
74.2	9.8
68.5	12.3
62.6	15.05
57.0	17.9
51.3	21.0
45.6	24.3
39.8	27.7
34.0	31.2
28.5	34.8
22.7	38.7
16.98	42.6